Development/Plasticity/Repair

Functional Cooperation of α-Synuclein and Tau Is Essential for Proper Corticogenesis

Shengming Wang,[1] Yu Fu,[1] Takaki Miyata,[2] Sakiko Matsumoto,[1] Tomoyasu Shinoda,[2] Kyoko Itoh,[3] Akihiro Harada,[4] Shinji Hirotsune,[1] and Mingyue Jin[1,5]

[1]Department of Genetic Disease Research, Osaka Metropolitan University Graduate School of Medicine, Osaka 545-8585, Japan, [2]Department of Anatomy and Cell Biology, Nagoya University Graduate School of Medicine, Nagoya 466-8550, Japan, [3]Department of Pathology and Applied Neurobiology, Graduate School of Medical Science, Kyoto Prefectural University of Medicine, Kyoto 602-8566, Japan, [4]Department of Cell Biology, Graduate School of Medicine, Osaka University, Osaka 565-0871, Japan, and [5]Guangxi Key Laboratory of Brain and Cognitive Neuroscience, Guilin Medical University, Guilin, Guangxi 541199, China

Alpha-synuclein (αSyn) and tau are abundant multifunctional neuronal proteins, and their intracellular deposits have been linked to many neurodegenerative diseases, including Alzheimer's disease and Parkinson's disease. Despite the disease relevance, their physiological roles remain elusive, as mice with knock-out of either of these genes do not exhibit overt phenotypes. To reveal functional cooperation, we generated $\alpha Syn^{-/-}tau^{-/-}$ double-knock-out mice and characterized the functional cross talk between these proteins during brain development. Intriguingly, deletion of αSyn and tau reduced Notch signaling and accelerated interkinetic nuclear migration of G2 phase at early embryonic stage. This significantly altered the balance between the proliferative and neurogenic divisions of progenitor cells, resulting in an overproduction of early born neurons and enhanced neurogenesis, by which the brain size was enlarged during the embryonic stage in both sexes. On the other hand, a reduction in the number of neural progenitor cells in the middle stage of corticogenesis diminished subsequent gliogenesis in the $\alpha Syn^{-/-}tau^{-/-}$ cortex. Additionally, the expansion and maturation of macroglial cells (astrocytes and oligodendrocytes) were suppressed in the $\alpha Syn^{-/-}tau^{-/-}$ postnatal brain, which in turn reduced the male $\alpha Syn^{-/-}tau^{-/-}$ brain size and cortical thickness to less than the control values. Our study identifies important functional cooperation of αSyn and tau during corticogenesis.

Key words: alpha-synculein; corticogenesis; gliogenesis; neurogenesis; tau

Significance Statement

Correct understanding of the physiological functions of αSyn and tau in CNS is critical to elucidate pathogenesis involved in the etiology of neurodegenerative diseases including Alzheimer's disease and Parkinson's disease. We show here that αSyn and tau are cooperatively involved in brain development via maintenance of progenitor cells. αSyn and tau double-knock-out mice exhibited an overproduction of early born neurons and accelerated neurogenesis at early corticogenesis. Furthermore, loss of αSyn and tau also perturbed gliogenesis at later embryonic stage, as well as the subsequent glial expansion and maturation at postnatal brain. Our findings provide new mechanistic insights and extend therapeutic opportunities for neurodegenerative diseases caused by aberrant αSyn and tau.

Received Feb. 26, 2022; revised July 7, 2022; accepted July 21, 2022.

Author contributions: S.H., and M.J. designed research; S.W., Y.F., T.M., S.M., T.S., A.H., S.H., and M.J. performed research; S.M. and K.I. contributed unpublished reagents/analytic tools; S.W., Y.F., S.M., and M.J. analyzed data; and S.H. and M.J. wrote the paper.

This work was supported by Japan Society for the Promotion of Science Grants JP17H04047 to S.H., JP18K06936 and JP21K06821 to M.J., and JP19K16525 and JP22K06887 to S.M, and Japan Agency for Medical Research and Development Grant JP18ek0109390 to S.H., M.J., and S.M. This work was also supported by the Natural Science Foundation of Guangxi Province (No. 2022GXNSFAA035622 to M.J.). We thank Miyuki Kira (Osaka Metropolitan University) and Yoriko Yabunaka (Osaka Metropolitan University) for technical support of DNA sequencing and HPLC analysis, Hiromichi Nishimura (Osaka Metropolitan University) and Junko Hirohara (Osaka Metropolitan University) for mouse breeding, the Osaka Metropolitan University Graduate School of Medicine for results data that were partially obtained using the Research Support Platform, Dr. Ayano Kawaguchi for data analysis and discussion (Nagoya University), and Namiko Noguchi (Nagoya University) and Makoto Masaoka (Nagoya University) for *in utero* electroporation.

The authors declare no competing financial interests.

Correspondence should be addressed to Shinji Hirotsune at shinjih@omu.ac.jp or Mingyue Jin at jinmingyue@omu.ac.jp.

https://doi.org/10.1523/JNEUROSCI.0396-22.2022

Introduction

Alpha-synuclein (αSyn) and tau are typically characterized as intrinsically disordered proteins (Weinreb et al., 1996; Chang et al., 2021) and are implicated in various neurodegenerative diseases, including Alzheimer's disease (AD; Chang et al., 2021) and Parkinson's disease (PD; Polymeropoulos et al., 1997). Tau is a major neuronal microtubule-associated protein (MAP) abundantly expressed in neuronal axons (Cleveland et al., 1977; Drubin and Kirschner, 1986), whereas αSyn is a synaptic protein highly concentrated in nerve terminals (Maroteaux et al., 1988). Previous studies have also revealed that αSyn and tau promote and stabilize microtubule (MT) polymerization (Alim et al., 2004; Qiang et al., 2006; Cartelli et al., 2016; Toba et al., 2017). Consistent with these effects, intracellular deposition of αSyn

and tau disrupts neuronal MTs (Chen et al., 2007) and impairs axonal transport (Calogero et al., 2019), common features in many neurodegenerative disorders in early onset individuals (Millecamps and Julien, 2013; Prots et al., 2018).

Neuronal MTs are essential for cell morphology, neurodevelopment, maintenance of physiological functions, and axonal transport (Sleigh et al., 2019). Hence, mutations in tubulins or MAPs have been linked to neurodevelopmental (Poirier et al., 2007; Jin et al., 2017) and neurodegenerative disorders (Calogero et al., 2019; Shafiq et al., 2021). Unexpectedly, although αSyn and tau are expressed throughout brain development (Hsu et al., 1998; Fiock et al., 2020), neither αSyn-deficient (Abeliovich et al., 2000) nor tau-deficient (Harada et al., 1994; Ke et al., 2012) mice showed clear phenotypes during brain development. These findings indicate the possibility of some functional redundancy among neuronal MAPs (Harada et al., 1994). Interestingly, αSyn and tau are codeposited in multiple neurodegenerative diseases, such as AD, dementia with Lewy bodies, and PD (Forman et al., 2002; Ishizawa et al., 2003; Moussaud et al., 2014). These findings strongly demonstrate that αSyn and tau play important roles in both cognition and movement. To exclude functional redundancy and clarify the functional cross talk between αSyn and tau, we crossed two single-knock-out (single-KO) strains to generate $\alpha Syn^{-/-}tau^{-/-}$ double-KO mice. We hypothesized that simultaneous deletion of two neuronal MAPs, αSyn and tau, may affect embryonic brain development, probably because of disruption of MT behaviors.

During mammalian corticogenesis, two kinds of neural progenitor cells (NPCs) radial glial cells (RGCs) and intermediate progenitor cells (IPCs) are present in the ventricular zone (VZ) and subventricular zone (SVZ), respectively (Greig et al., 2013). These cells proliferate and give rise to postmitotic neurons. The coordinated proliferation and differentiation of NPCs and neuronal migration play a pivotal role in creating a highly organized brain structure and proper neuronal networks (Taverna et al., 2014). In this study, we investigated the cooperative functions of αSyn and tau during brain development by dissecting $\alpha Syn^{-/-}tau^{-/-}$ mice. Surprisingly, compared with the wild-type (WT) strain and the two single-KO strains, the $\alpha Syn^{-/-}tau^{-/-}$ mice had smaller brains, suggesting the presence of microcephaly in the adult mice. In contrast, NPCs from $\alpha Syn^{-/-}tau^{-/-}$ mice exited the cell cycle prematurely at embryonic day (E)11 and displayed facilitated neurogenesis from E12 that led to an enlarged brain during the embryonic stage. We also found that $\alpha Syn^{-/-}tau^{-/-}$ mice showed diminished gliogenesis at the late embryonic stage and subsequent expansion and maturation in the postnatal brain. Moreover, this downregulated gliogenesis, expansion, and maturation led to the reduced brain size in $\alpha Syn^{-/-}tau^{-/-}$ mice compared with WT and single-KO mice. Together, these findings indicate that functional cooperation between αSyn and tau plays multiple roles in different developmental processes.

Materials and Methods

All methods were performed in accordance with the approved guidelines. All experimental protocols were approved by the Osaka Metropolitan University Graduate School of Medicine. Separate approval was provided for the recombinant DNA experiments (Osaka Metropolitan University no. 708) and animal experiments (Osaka Metropolitan University no. 21094).

Animal sources and maintenance . Both sexes of mouse embryos and pups were used at E11–E15 and postnatal day (P)0–P11, respectively; and adult male mice were used at 6 weeks of age, as indicated in the main text and figures. Homozygous α-synuclein (αSyn) KO mice (B6;129 × 1-*Snca*^{tm1Rosl}/J, strain #003692) were purchased from The Jackson Laboratory, and heterozygous tau KO mice (B6;129-*Mapt* $^{tm1(Cre)}$) were generated by Akihiro Harada (Department of Cell Biology, Graduate School of Medicine, Osaka University) and housed in the Center for Animal Resources and Development, Kumamoto University. In this study, mice were maintained on a C57BL/6 background, WT C57BL/6 mice were used as controls, and homozygous $\alpha Syn^{-/-}$, $tau^{-/-}$ and $\alpha Syn^{-/-}tau^{-/-}$ mice were used as experimental mice. All mice were housed in an environmentally controlled room in the Institute of Laboratory Animals of the Graduate School of Medicine, Osaka Metropolitan University. Each cage contained fewer than six mice, and mice were provided access to food and water *ad libitum*.

Generation of double-knock-out mice. αSyn and tau double knockout mice were generated by crossing $\alpha Syn^{-/-}$ and $tau^{-/-}$ mice. Genotyping was performed by standard PCR, with denaturation at 94°C for 1 min followed by 35 cycles of denaturation at 94°C for 20 s, annealing at 55°C for 30 s, and extension at 72°C for 1 min. The following primers were used: Tau forward (F), 5′-TATGGCTGACCCTCGCCAGGAGTTT-3′; Tau reverse (R), 5′-TCCACCCCACTGACCTTTTAAGCC-3′; αSyn F, 5′-ATGGATGTGTTCATGAAAGGACTTTCAA-3′; and αSyn R, 5′-ACTTCCCAAATGCCACCAGGC-3′.

Calculation of brain surface area. Mice at E14, P11, and 6 weeks were chosen for calculation of the brain surface area. Samples were harvested in PBS at 4°C, and images were acquired using optical microscope (Olympus BX53) at 1.25× or 2× magnification. The surface areas were circled in the images and calculated with Fiji ImageJ software.

Sectioning of brain samples. Embryos were sacrificed and dissected in PBS and then fixed with periodate-lysine-paraformaldehyde (PLP) at 4°C for 2 h (E11–E13 embryos), 3 h (E14 embryos) and 5 h (E15 embryos). Pups and adult mice were perfused with PLP solution (P0, 5 ml/pup; P7 and P11, 15 ml/pup; 6 weeks old, 60 ml/mouse), and the brains were fixed by continuous incubation in PLP overnight at 4°C. For sectioning, samples were washed in PBS, cryoprotected in 20% sucrose/PBS overnight at 4°C, embedded in optimal cutting temperature compound and sliced at a 16 μm thickness on a Leica CM 1950 cryostat. Nissl staining of sections was performed with 0.25% thionin acetate salt (catalog #861340, Sigma-Aldrich).

Immunohistochemistry. Brain sections were washed in PBS and subjected to antigen retrieval in 10 mM citrate buffer, pH 6.0, for 10–15 min at ~80°C. After washing, the sections were blocked in 1% BSA supplemented with 0.1% Triton X-100, 0.01% NaN_3, and primary antibodies overnight at 4°C. The primary antibodies used in this study included mouse anti-Pax6 (1:200; catalog #ab78545, Abcam), rabbit anti-Pax6 (1:200; catalog #901301, BioLegend), rabbit anti-Tbr2 (1:500; catalog #ab23345, Abcam), rabbit anti-Tbr1 (1:500; catalog #ab31940, Abcam), rabbit anti-Ki67 (1:200; catalog #ab16667, Abcam), mouse anti-glial fibrillary acidic protein (GFAP; 1:500; catalog #G3893, Sigma-Aldrich), mouse anti-Olig2 (1:500; catalog #MABN50, Millipore), rabbit anti-Cux1 (1:500, catalog #sc-13024, Santa Cruz Biotechnology), rat anti-Ctip2 (1:200; catalog #ab18465, Abcam), mouse anti-S100β (1:500; catalog #AMAb91038, Sigma-Aldrich), mouse anti-neurogenin 2 (Ngn2; 1:200; catalog #MAB3314, R&D Systems), mouse anti-Ascl1 (1:200; catalog #556604, BD Biosciences), rabbit anti-Notch1 (1:100; catalog #3608, Cell Signaling Technology), rat anti-5-Bromo-2′-deoxyuridine (BrdU; 1:100; catalog #ab6326, Abcam), rabbit anti-cleaved caspase-3 (1:200; catalog #966, Cell Signaling Technology), and rabbit anti-Iba1 (1:1000; catalog #019-19741, Waco) antibodies. The secondary antibodies, including Alexa Fluor 488-conjugated antibodies (goat anti-mouse IgG, catalog #A11001; goat anti-rabbit IgG, catalog #A11008; goat anti-rat IgG, catalog #A11006, Invitrogen) and Alexa Fluor 546-conjugated antibodies (goat anti-mouse IgG, catalog #A11003; goat anti-rabbit IgG, catalog #A11010; goat anti-rat IgG, catalog #A11081, Invitrogen) were diluted 1:500 in blocking buffer. The brain sections were also stained with 4′,6′-diamidino-2-phenylindole (DAPI; 1:500; catalog #D523, Dojindo) for 2 h at room temperature (RT) in the dark and mounted with FluorSave Reagent (catalog #345789, Millipore). Images were acquired using an LSM800 laser confocal microscope (Zeiss) with a 40× or water-immersion 63× objective lens.

BrdU treatment. BrdU (catalog #B9285, Sigma-Aldrich) was injected intraperitoneally into mice (50 μg/g mouse weight), and the mice were housed in a temperature-controlled room with access to food and water *ad libitum* until they were sacrificed. For BrdU staining, brain sections were subjected to antigen retrieval with 2 N HCl for 10 min, washed with PBS, and incubated with primary antibodies.

RNA preparation and qRT-PCR. Total RNA samples were extracted from nine of E12 embryonic cortices/genotype using an RNeasy Plus Mini Kit (QIAGEN) and reversely transcribed into cDNA with SuperScript Reverse Transcriptase III (Invitrogen) and nucleotide oligo-dT primers. Quantitative PCR (qPCR) was performed on a QuantStudio 5 Real-Time PCR System (Applied Biosystems) using PowerUp SYBR Green Master Mix (Applied Biosystems). The following primers were used: Notch1 F, 5′-GGTGAACAATGTGGATGCTG-3′; Notch1 R, 5′-ACTTTGGCAGTCTCATAGCTG-3′; β-actin F, 5′-GCCTTCCTTCT TGGGTATG-3′; and β-actin R, 5′-ACCACCAGACAGCACTGTG-3′.

Cell culture. Mouse embryonic fibroblasts (MEFs) were separated from embryos (E12–E13) and cultured in high glucose D-MEM (catalog #043-30085, Wako), supplemented with 10% FBS (catalog #171012, NICHIREI BIOSCIENCES INC), 1× L-glutamine (catalog #25030-081, Invitrogen,) and 1× antibiotic mixture (penicillin-streptomycin solution, catalog #168-23191, Wako). To assess microtubule reorganization, MEFs were cultured on poly-L-lysine (PLL)-precoated coverslips in six-well plates and incubated with nocodazole (at concentrations of 0, 1, and 2 μg/ml in D-MEM) for 1 h at RT. Then the cells were rinsed with PBS for subsequent immunostaining. Lenti-X 293T cells were cultured in high glucose D-MEM, supplemented with 5% FBS, 1× L-glutamine, and 1× antibiotic mixture for lentivirus preparation.

Western blot analysis. Brain neocortices dissected from E12 embryos were lysed in lysis buffer (T-PER Tissue Protein Extraction Reagent, catalog #78510, Thermo Scientific; 1× Protease Inhibitor Cocktail, #78425, Thermo Fisher Scientific; 5 mM EDTA; 1 mM DTT). For immunoblotting, proteins were separated on acrylamide gels under reducing conditions and were then electrophoretically transferred to PVDF membranes. The membranes were incubated with blocking buffer (5% skim milk in TBS-T) and were then probed with antibodies against Notch intracellular domain (NICD; 1:1000; catalog #ab52301, Abcam), Hes1 (1:1000; catalog #sc-166410, Santa Cruz Biotechnology), Hes5 (1:1000; catalog #ab25374, Abcam) and β-actin (1:1000; catalog #A2228, Sigma-Aldrich), followed by incubation with a horseradish peroxidase-conjugated secondary antibody at a 1:1000 dilution [Donkey Anti-Mouse IgG (H+L), catalog #715-035-150, Jackson ImmunoResearch; Donkey Anti-Rabbit IgG (H+L), catalog #711-035-152; Jackson ImmunoResearch]. Blots were developed using ECL Prime detection reagent (Cytiva), and chemiluminescence was detected with a FUSION Solo S imaging system (VILBER).

Immunocytochemistry. MEFs were fixed with prewarmed 4% paraformaldehyde (PFA; catalog #163-20145, Wako) for 15 min at 37°C, treated with 0.1% Triton X-100 for 5 min, and then blocked in 4% BSA before primary antibody treatment. The cells were incubated with rabbit anti-β-tubulin antibody (1:300; catalog #ab6046, Abcam) in blocking solution for 1 h at RT. An Alexa Fluor 546-conjugated secondary antibody (goat anti-rabbit IgG, 1:1000; catalog #A11010, Invitrogen) was used, and the nuclei were stained with DAPI (1:500; catalog #D523, Dojindo) for 1 h at RT in the dark. Images were acquired using an LSM700 confocal microscope (Zeiss) with a 20× objective lens.

Lentivirus preparation. Lentiviruses were prepared as described previously (Toba et al., 2017). Briefly, the EB3 cDNA fragment fused to mNeonGreen (mNG) was subcloned into the self-inactivating lentiviral vector pCSII-EF-MCS-IRES2, which was then cotransfected with the packaging plasmids pCAG-HIVgp and the VSV-G and Rev-expressing pCMV-VSV-G-RSV-Rev into Lenti-X 293T cells (5×10^6 n/p 10 dish) by using PEI MAX. After 48 h of culture, lentiviral particles were collected by ultracentrifugation at 17,000 rpm at 20°C for 2 h (CP80NX, P28S rotor, Himac). The pellet was then resuspended in 600 μl of PBS, aliquoted at 20 μl/tube, and stored at −80°C until use.

EB3 tracking analysis. MEF cells were cultured in PLL-precoated glass bottom dishes (35 mm, catalog #3910-035, Iwaki) and induced to overexpress EB3-mNG via lentivirus transduction (4 μl/dish, 48 h). Live cell images were recorded with an Olympus IX70 microscope coupled to a digital charge-coupled device (CCD) camera (EM-CCD C9100-13, Hamamatsu Photonics) with an oil immersion objective lens (Plan Apo 60×, numerical aperture 1.40, Nikon Instech) and Aqua Cosmos 2.6 software (Hamamatsu Photonics). Moving EB3 particles were tracked using Mark2 tracking software (provided by Ken'ya Furuta).

In utero electroporation and slice culture. In utero electroporation (IUE) was performed using pregnant WT and $\alpha Syn^{-/-}tau^{-/-}$ mice as previously described (Okamoto et al., 2013; Shinoda et al., 2018) with minor modifications. Approximately 1 μl of the plasmid mixture (pEF1α-Cre, pEF1α-LPL-Lyn-EGFP, and pBA-LPL-H_2B-RFP with 0.02% Fast Green) was injected into the lateral ventricle of each intrauterine E12 embryo. Then, the head of each embryo was placed between the disks of a forceps-type electrode (3 mm disk electrode, model CUY650P3, NEPA GENE), and the genes were electroporated into the cerebral walls by electronic pulses (30–50 V, 50 ms, five times). At E13 (or E14), coronal cerebral wall slices prepared at a 200–250 μm thickness were embedded in type I collagen gel in a 35 mm glass bottom dish (Iwaki), and live images were recorded with a CellVoyager CV1000 microscope system (Yokogawa Electric) at 10 min intervals.

Quantification and statistical analyses. All experimental data presented here were obtained from at least three independent replicates, and analyses were performed with blinding to the genotype or condition. Cells were counted in a 100 μm column for E11–E15 cortices and in a 300 μm column for P0, P7, P11, and 6-week-old cortices; neuronal cell densities were calculated in a 100 × 100 μm^2 area for P7, P11, and 6-week-old cortices with ZEN software (Zeiss; details provided in each figure legend). For comparisons between two or more groups, unpaired two-tailed Student's *t* tests or one-way ANOVA followed by Tukey's *post hoc* test, respectively, were used to calculate *p* values. Significance was set at $p < 0.05$, and the data are presented as mean ± SEM; $^*p < 0.05$, $^{**}p < 0.01$, $^{***}p < 0.001$.

Results

Generation of $\alpha Syn^{-/-}tau^{-/-}$ double-knock-out mice

Although αSyn and tau are highly abundant MAPs expressed throughout brain development (Hsu et al., 1998; Fiock et al., 2020), mice with single-KO of either gene do not display overt phenotypes (Ke et al., 2012; Pathak et al., 2017), indicating the existence of some degree of functional redundancy among neuronal MAPs. To eliminate this functional redundancy and address the functional cross talk between αSyn and tau, we generated $\alpha Syn^{-/-}tau^{-/-}$ double-KO mice by crossing $\alpha Syn^{-/-}$ mice (Abeliovich et al., 2000) with $tau^{-/-}$ mice (Muramatsu et al., 2008; Fig. 1*A*). $\alpha Syn^{-/-}tau^{-/-}$ mice were viable and fertile, and survived to adulthood. Both male and female $\alpha Syn^{-/-}tau^{-/-}$ mice had normal body sizes and weights relative to those of WT and single-KO (either $\alpha Syn^{-/-}$ or $tau^{-/-}$) littermates and did not exhibit any obvious morphologic defects. We first examined the brain structure at 6 weeks after birth. We found clear reductions in brain size in 6-week-old $\alpha Syn^{-/-}tau^{-/-}$ mice (Fig. 1*B*,*C*). In addition, the cortical layers and thickness were assessed after immunolabeling with the markers Cux1 (layers II–IV) and Ctip2 (layers V–VI; Nieto et al., 2004; Arlotta et al., 2005). Although, the thickness of layers II–VI was significantly decreased in $\alpha Syn^{-/-}tau^{-/-}$ mice (Fig. 1*D*,*E*), the numbers of neurons in each layer probed with Cux1 and Ctip2 were unaffected (Fig. 1*D*,*F*,*G*). These results strongly suggest that αSyn and tau play essential roles during brain development.

Deletion of αSyn and tau promotes neurogenesis

Corticogenesis depends on the highly regulated proliferation and differentiation of NPCs. To examine the effects of αSyn and tau during brain development, we first assessed the behavior of cortical NPCs at E14, a middle stage of corticogenesis. In contrast to

the small brains observed at 6 weeks, the brains of $\alpha Syn^{-/-}tau^{-/-}$ mice at E14 were significantly larger than those of WT and single-KO mice (Fig. 2*A*). This result further indicated that abnormalities occurred during the proliferation and differentiation of RGCs in $\alpha Syn^{-/-}tau^{-/-}$ mice. Next, we assessed proliferative RGCs using the S phase marker BrdU and the cycling cell marker Ki67 at E14. Two hours after peritoneal injection of BrdU, brain samples were collected, and the sections were stained with antibodies against BrdU and Ki67 (Fig. 2*B*, *C*). Despite the brain enlargement observed at E14, the number of BrdU+Ki67+ cycling NPCs was clearly reduced in $\alpha Syn^{-/-}tau^{-/-}$ mice (Fig. 2*C*). However, the numbers of Pax6+ RGCs did not differ among the WT and KO mice (Fig. 2*D*,*E*). On the other hand, the number of Tbr2+ IPCs was significantly reduced in $\alpha Syn^{-/-}tau^{-/-}$ cortices (Fig. 2*D*,*F*,*G*). Interestingly, we also found that the numbers of differentiated neurons as identified by the DAPI+Pax6-Tbr2- were remarkably increased in the VZ and SVZ in $\alpha Syn^{-/-}tau^{-/-}$ mice (Fig. 2*D*, *H*). These findings showed that although the number of IPCs was decreased, neurogenesis was remarkably enhanced by deletion of αSyn and tau. Consistent with this finding, the number of Tbr1+ postmitotic neurons was remarkably increased in the $\alpha Syn^{-/-}tau^{-/-}$ cortical plate (CP), accompanied by an apparent increase in CP thickness (Fig. 2*I*). These data indicated that the promotion of neurogenesis was concomitant with increases in the cortical thickness and brain size. We further examined the NPC pool at E15 and found that the numbers of both RGCs and IPCs were significantly decreased in $\alpha Syn^{-/-}tau^{-/-}$ cortices (Fig. 2*J*–*M*), suggesting that the promotion of neurogenesis led to excess consumption of RGCs and consequently reduced the number of NPCs.

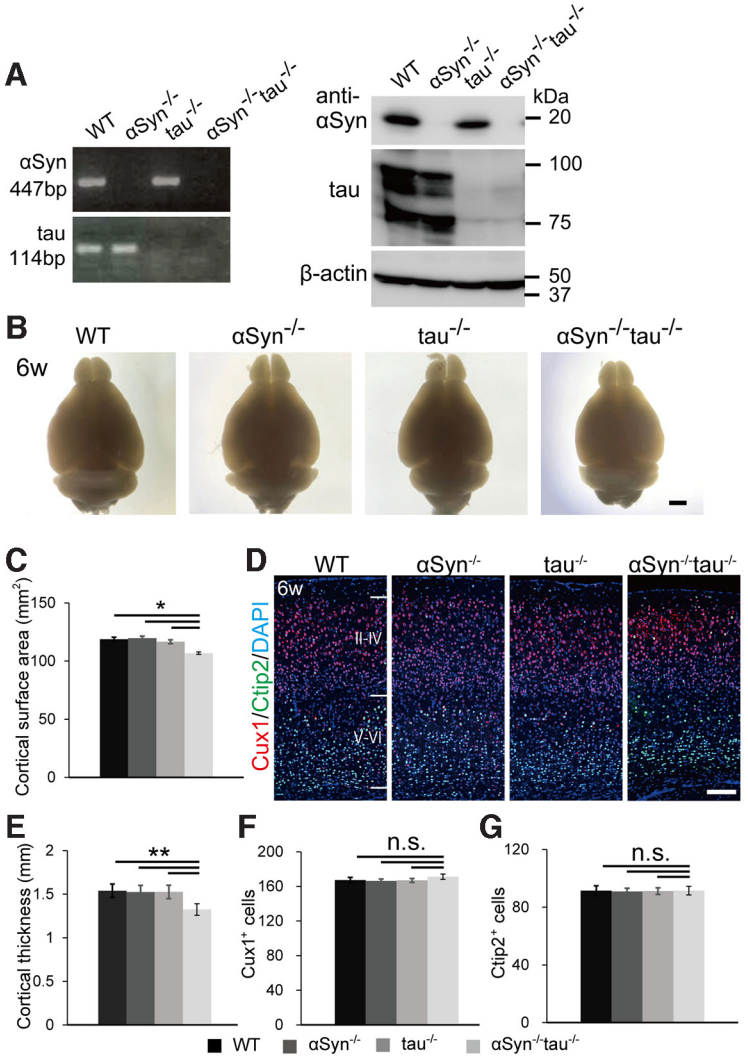

Figure 1. Loss of αSyn and tau reduced the brain size in adult mice. ***A***, Generation of $\alpha Syn^{-/-}tau^{-/-}$ mice by crossing $\alpha Syn^{-/-}$ mice with $tau^{-/-}$ mice. $\alpha Syn^{-/-}tau^{-/-}$ mice were confirmed by genotyping (left) and Western blotting (right). ***B***, ***C***, Comparison of cortical surface areas in 6-week-old (6w) WT and KO mice. Scale bar, 2 mm. ***D–G***, Cortical architecture in 6-week-old mice, as visualized with antibodies against Cux1 (layers II–IV, red) and Ctip2 (layers V–VI, green). The thickness of cortical layers II–VI (***E***) and the numbers of Cux1+ upper layer neurons (***F***) and Ctip2+ deep layer neuronal cells (***G***) were quantified in WT and KO mice. In this study, cell nuclei were stained with DAPI (blue). Scale bar, 200 μm. The quantitative data are presented as mean ± SEM, $N = 3$ mice per genotype from three separate litters. The p values were calculated by one-way ANOVA with Tukey's *post hoc* test; n.s., not significant; *$p < 0.05$, **$p < 0.01$.

Loss of αSyn and tau induces premature neurogenesis

In E14 $\alpha Syn^{-/-}tau^{-/-}$ brains, despite the increased numbers of postmitotic neurons and the thickened CP, differentiation to IPCs was diminished probably because of the promotion of direct neurogenesis from RGCs. To address the origin of the conflicting data at E14, we performed analyses at E12, an earlier stage of neurogenesis, and the time at which the RGC-IPC-neuron differentiation system is initiated (Bond et al., 2020). As expected, immunohistochemistry revealed that the number of cycling RGCs (Pax6+Ki67+) was significantly increased in E12 $\alpha Syn^{-/-}tau^{-/-}$ brains (Fig. 3*A*,*B*). This increase may have contributed to the maintenance of the RGC pool until E14. To trace differentiation, we labeled mitotic NPCs with BrdU at E12 and the mice were sacrificed after 24 h (Fig. 3*C*). Brain sections were stained with antibodies against BrdU, Ki67, and Tbr1. Compared with WT and both types of single-KO cortices, $\alpha Syn^{-/-}tau^{-/-}$ cortices displayed increases in the numbers of both mitotic progenitors (BrdU+Ki67+; Fig. 3*D*,*E*) and cell cycle-exiting neurons (BrdU+Ki67-/BrdU+; Fig. 3*D*,*F*). Consistently, the number of postmitotic neurons identified by either Tbr1+ or BrdU+Tbr1+/BrdU+ was clearly increased in the $\alpha Syn^{-/-}tau^{-/-}$ neocortex (Fig. 3*G*–*I*). Unexpectedly, we found that postmitotic neurons probed with antibody specific for the deep layer marker Ctip2 were detected only in E11 $\alpha Syn^{-/-}tau^{-/-}$ mice, strongly indicating that loss of αSyn and tau functions resulted in precocious neurogenesis from E11 (Fig. 3*J*,*K*)

Next, we investigated the differentiation of RGCs to IPCs at E12. In contrast to the findings at E14, the number of Tbr2+ IPCs was increased significantly in the $\alpha Syn^{-/-}tau^{-/-}$ group (Fig. 4*A*,*B*), suggesting that enhanced proliferation and differentiation of RGCs occurred from E12. Ngn2, another IPC marker, is the main determinant of cortical neuronal fate (Miyata et al., 2004; Kawaguchi et al., 2008; Han et al., 2018). Consistent with the data shown in Figure 4, *A* and *B*, the number of Ngn2+ IPCs was also increased in the $\alpha Syn^{-/-}tau^{-/-}$ group (Fig. 4*C*,*D*). These

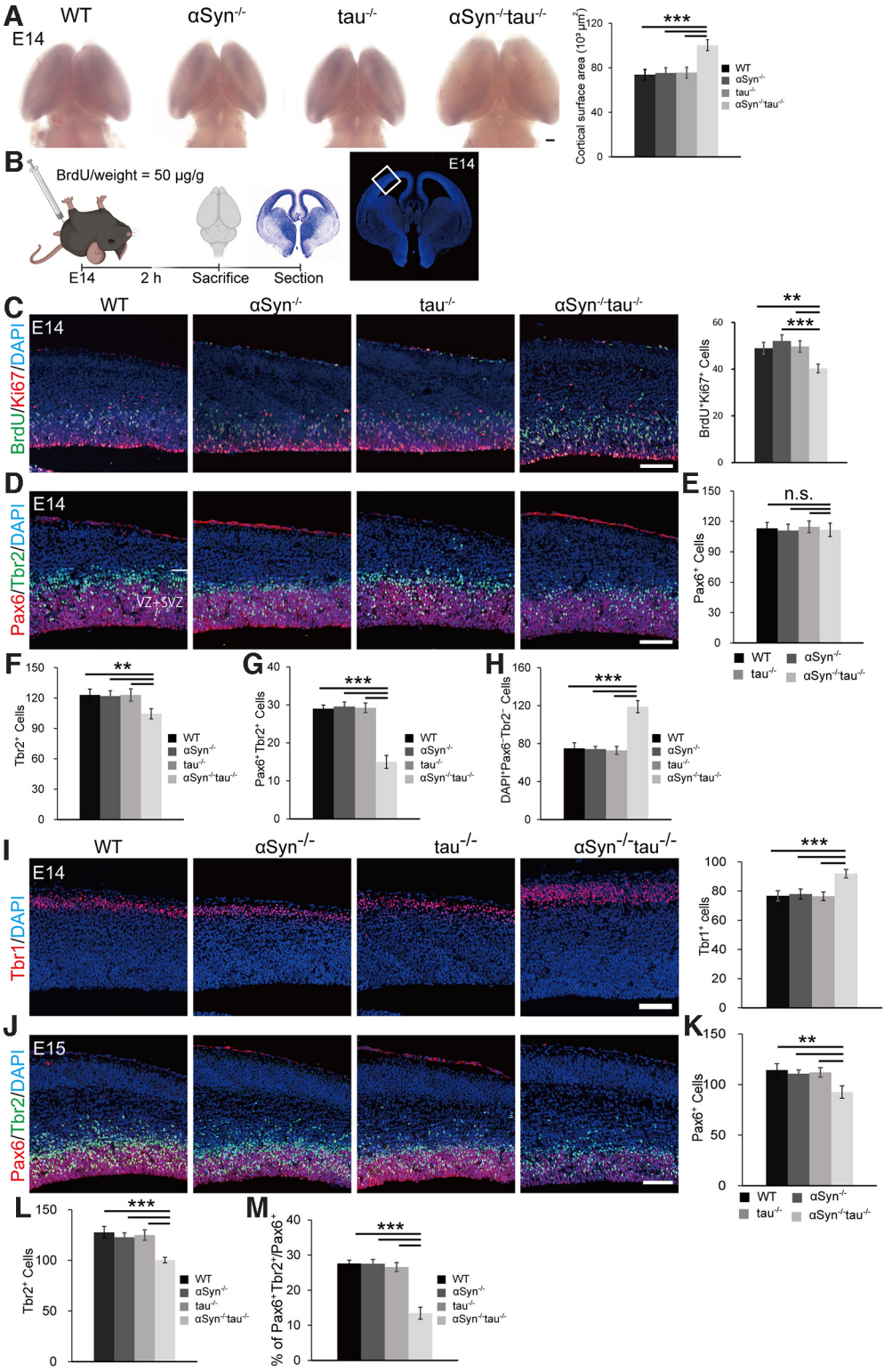

Figure 2. Loss of αSyn and tau promoted neurogenesis. ***A***, Comparison of cortical surface areas at E14. Scale bar, 200 μm. ***B***, Schematic illustration of the BrdU experiments and the image acquisition area as indicated in the white rectangle. ***C***, Analyses of cycling NPCs after BrdU injection at E14. Two hours after BrdU injection, brain sections were stained with anti-BrdU (S phase marker, green) and anti-Ki67 (cycling cell marker, red) antibodies, and cycling NPCs in the VZ and SVZ were quantified. BrdU+Ki67+ cells were counted in 100 μm columns in sections from each genotype. Scale bar, 50 μm. ***D–H***, Quantification of the NPC pool and generated neurons at E14 by immunostaining for the RGC marker Pax6 (red) and the IPC marker Tbr2 (green). Representative immunostaining images are shown in (***D***). NPCs were probed with Pax6 and/or Tbr2 markers (***D–G***), and the generated neurons identified by the DAPI+Pax6-Tbr2- (***H***) in the VZ and SVZ were counted per 100 μm column for each genotype. Scale bar: (in ***D***) ***D–H***, 50 μm. ***I***, Statistical analysis of postmitotic neurons in the neocortex after probing with Tbr1. The cells were counted in a 100 μm column. ***J–M***, Quantification of NPCs in E15 cortices. RGCs and IPCs at E15 were stained with anti-Pax6 (red) and anti-Tbr2 (green) antibodies, respectively, and representative images are shown in ***J***. The quantitative RGCs and/or IPCs are shown in ***K–M***. The quantified data are presented as mean ± SEM, $N = 3$ embryos per genotype from three separate litters. The p values were calculated by one-way ANOVA with Tukey's *post hoc* test; n.s., not significant; $^{**}p < 0.01$, $^{***}p < 0.001$.

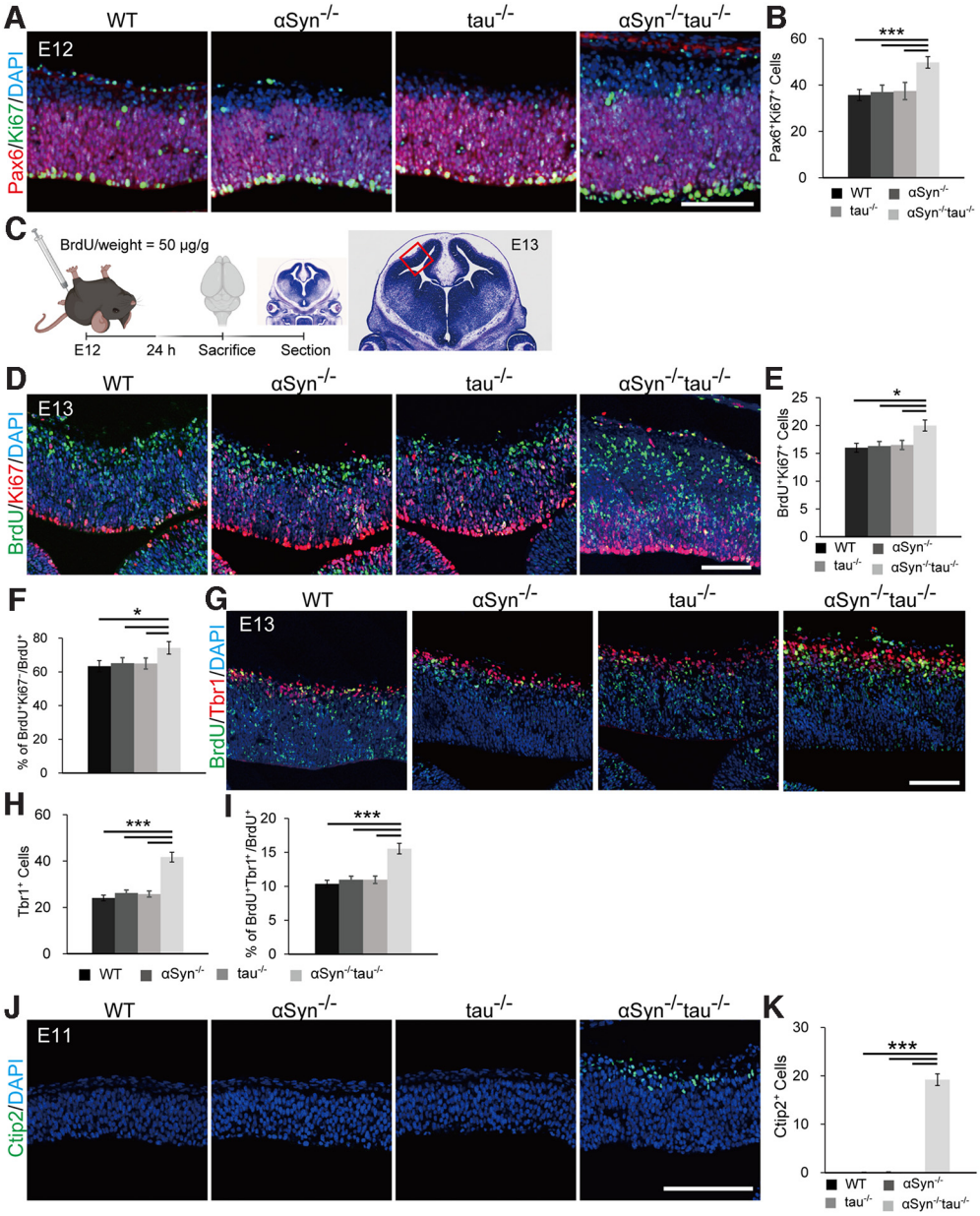

Figure 3. Proliferation and differentiation of RGCs were facilitated in $\alpha Syn^{-/-}tau^{-/-}$ E12 cortices. ***A***, ***B***, Statistical analyses of cycling RGCs in E12 cortices. Cycling RGCs were probed with antibodies against Pax6 (red) and Ki67 (green, ***A***), and the numbers of Pax6+ and Ki67+ cells were determined and are shown in ***B***. ***C–F***, Cell cycle exit assay during E12–E13. Schematic illustration of the BrdU experiments and the image acquisition area as indicated with the red rectangle (***C***). Representative images of E13 cortices after BrdU and Ki67 costaining are shown in ***D***. Statistical analyses of cycling cells (BrdU+Ki67+, ***E***) and cell cycle exiting cells (BrdU+Ki67-/BrdU+, ***F***) are presented. ***G–I***, Cycling cells were labeled with BrdU (green) at E12, and differentiated postmitotic neuronal cells were labeled with Tbr1 (red) at E13. Representative immunostaining images are shown in ***G***, and the postmitotic neurons were counted in 100 μm columns and are shown in ***H*** and ***I***. ***J***, ***K***, Premature neurogenesis caused by deletion of αSyn and tau. Differentiated neurons were probed with an anti-Ctip2 antibody (green, ***J***) and quantified (***K***). Cell counting was performed in 100 μm columns for each genotype. The data are presented as mean ± SEM, $N = 3$ embryos per genotype from three separate litters. The p values were calculated by one-way ANOVA with Tukey's *post hoc* test; *$p < 0.05$, ***$p < 0.001$. Scale bars: ***A*** (for ***A***, ***B***,) ***D*** (for ***C–F***), ***G*** (for ***G–I***), and ***J*** (for ***J***, ***K***), 50 μm.

IPCs are committed to differentiation into postmitotic neurons. Together, these results suggest that enhanced neurogenesis is induced by both RGCs and IPCs.

Considering the importance of the Notch signaling pathway in the maintenance of RGCs and neuronal differentiation (Kopan and Ilagan, 2009), we investigated Notch1 expression at E12. Notch1 was observed mainly in the VZ and SVZ in all tested E12 cortices, but the intensity of Notch1 immunofluorescence was apparently decreased in $\alpha Syn^{-/-}tau^{-/-}$ cortices (Fig. 4*E*,*F*), indicating reduced expression and impaired activity of Notch1. To confirm this, we also performed qPCR and found that the mRNA level of Notch1 in E12 $\alpha Syn^{-/-}tau^{-/-}$ mice was clearly lower than that in WT and both types of single-KO mice (Fig. 4*G*). Activation of Notch1 triggers the cleavage of the NICD, which then translocates to the nucleus to induce the expression of Hes proteins, ultimately inhibiting neuronal differentiation (Kopan and Ilagan, 2009). Western blot analysis revealed that the expression levels of NICD and its downstream Hes1 and Hes5 were remarkably decreased in E12 $\alpha Syn^{-/-}tau^{-/-}$ cortices (Fig. 4*H*,*I*). The increased number of Ngn2+ IPCs in $\alpha Syn^{-/-}tau^{-/-}$ cortices also supported this finding. These results indicate that the acceleration of neurogenesis in $\alpha Syn^{-/-}tau^{-/-}$ mice is caused by downregulation of Notch signaling.

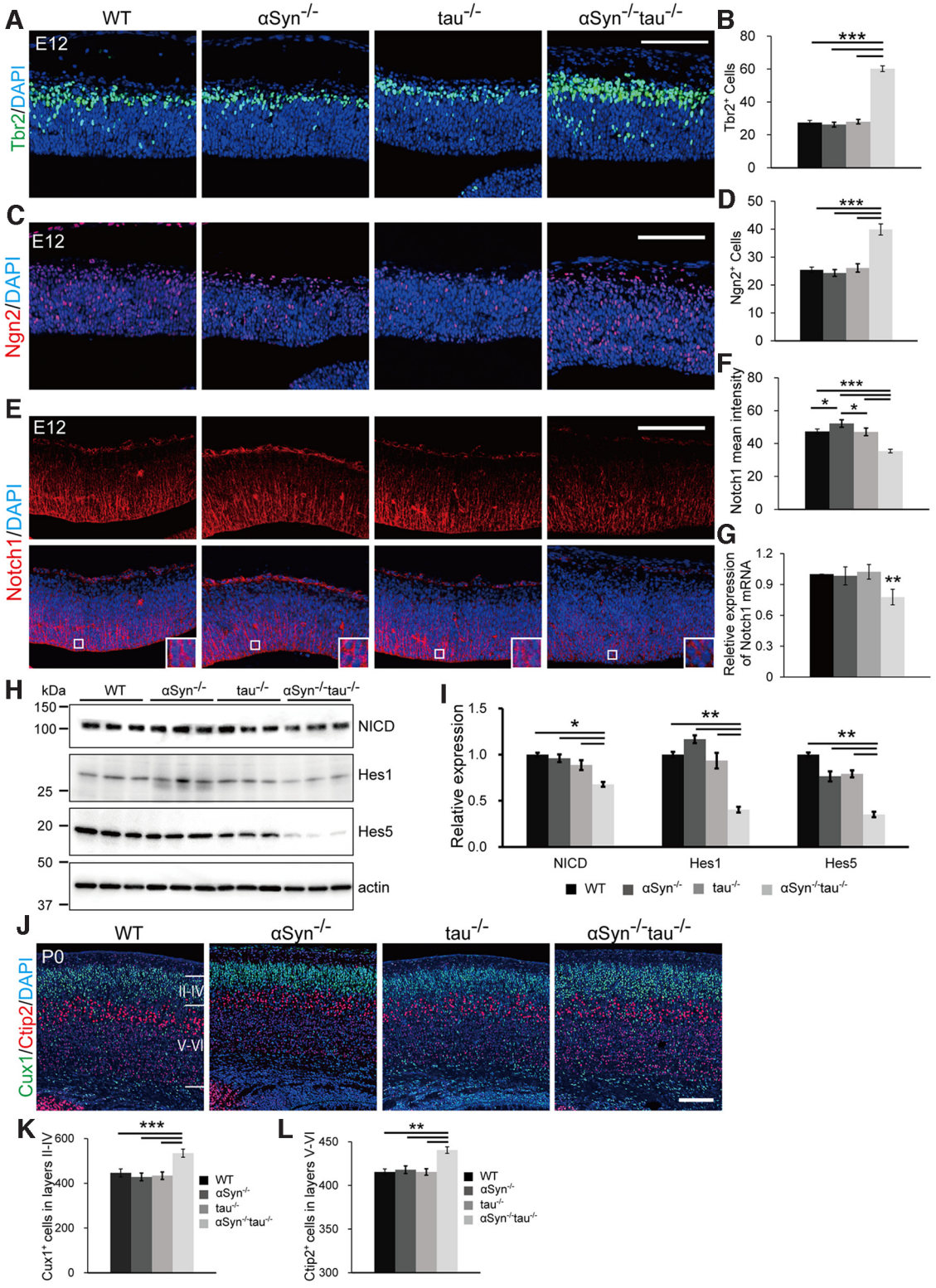

Figure 4. A reduction in Notch signaling promotes neurogenesis in $\alpha Syn^{-/-}tau^{-/-}$ E12 cortices. ***A***, ***B***, Differentiation of IPCs was examined with Tbr2, an IPC marker. Tbr2+ cells in the VZ and SVZ were quantified in 100 μm columns. ***C***, ***D***, Differentiation of IPCs was examined with the proneuronal marker Ngn2. Ngn2+ cells in the VZ and SVZ were quantified in 100 μm columns. ***E***, ***F***, Deletion of αSyn and tau led to a reduction in Notch1 expression in NPCs. Insets, Enlarged images from each boxed region. The mean Notch1 expression intensity in the VZ and SVZ was quantified. ***G***, Notch1 mRNA expression was quantified by qPCR. ***H***, ***I***, The expressions of NICD, Hes1, and Hes5 in E12 cortices were evaluated with Western blot analysis. The quantitative graphs are presented as means of triplicate values per genotype from three separate litters. ***J–L***, The P0 cortical architecture was visualized by staining for the layer markers Cux1 (green) and Ctip2 (red, ***J***), and the Cux1+ (***K***) and Ctip2+ (***L***) neurons were quantified per 300 μm column. The quantitative data are presented as mean ± SEM, $N = 3$ brains per genotype from three separate litters. Statistical analyses were performed with one-way ANOVA with Tukey's *post hoc* test; $^{*}p < 0.05$, $^{**}p < 0.01$, $^{***}p < 0.001$. Scale bars: (in ***A***) ***A***, ***B***, (in ***C***) ***C***, ***D***, and (in ***E***), ***E***, ***F***, 50 μm; (in ***J***) ***J–L***, 100 μm.

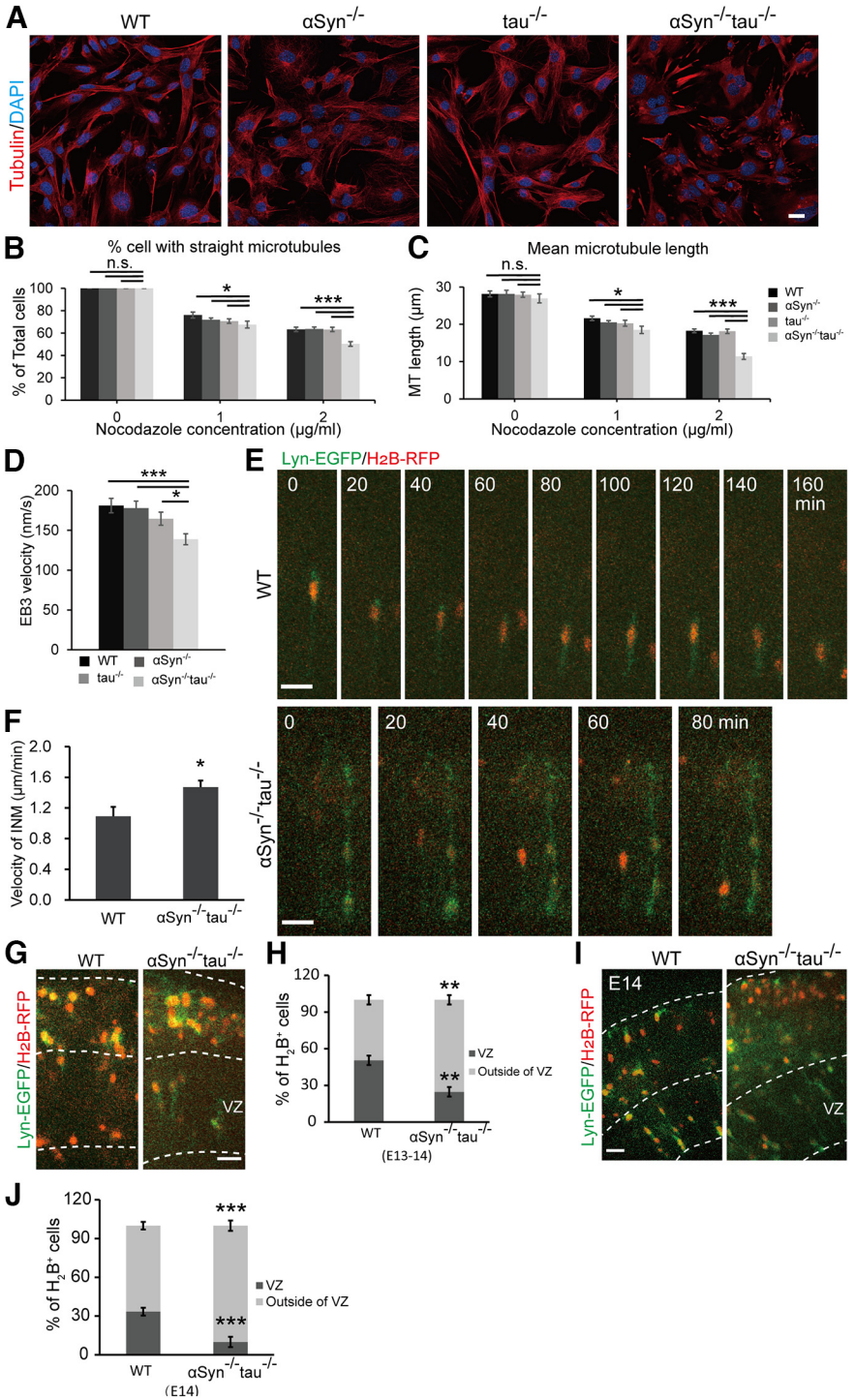

Figure 5. INM at the early embryonic stage was accelerated in αSyn$^{-/-}$tau$^{-/-}$ mice. ***A–C***, After nocodazole treatment, MEFs were stained with an anti-tubulin antibody (red, ***A***), and the number of cells with straight MTs (***B***) and the mean MT length (***C***) were determined; $N = 3$ repeats of independent experiments, 30 cells per genotype. ***D***, Quantified mean velocity of EB3-mNG particles in MEFs; $N = 3$ repeats of independent experiments, 30 particles from different cells per genotype. ***E***, ***F***, Apical movement of nuclei/somata during G2 phase in slice culture. After *in utero* electroporation of Lyn-EGFP (membrane, green) and H_2B-RFP (nuclei, red) at E12, E13 cerebral wall slices were observed (***E***), and the mean velocity of INM in G2 phase was quantified (***F***). At least 10 slices were observed, and 18 cells for the WT group and 33 cells for the αSyn$^{-/-}$tau$^{-/-}$ group were selected for INM quantification. ***G***, ***H***, After 16 h of observation of the cultured slices from ***E***, 49.5 and 75.3% of electroporated WT and αSyn$^{-/-}$tau$^{-/-}$ RGCs were found to have escaped from the VZ, respectively. For quantification, five slices for the WT and eight slices for the αSyn$^{-/-}$tau$^{-/-}$ were used. ***I***, ***J***, After IUE of Lyn-EGFP and H_2B-RFP at E12, slice culture was performed at E14. In electroporated cells, 66.5% of WT and 90% of αSyn$^{-/-}$tau$^{-/-}$ RGCs escaped from the VZ. For quantification, five slices for the WT and seven slices for the αSyn$^{-/-}$tau$^{-/-}$ were used. The data are presented as mean ± SEM, $N = 3$ brains from three different litters for each genotype. The p values were calculated by one-way ANOVA with Tukey's *post hoc* test or Student's t test; n.s., not significant; *$p < 0.05$, **$p < 0.01$, ***$p < 0.001$. Scale bars: (in ***A***) ***A–C***, 20 μm; (in ***E***) ***E***, ***F***, (in ***G***) ***G***, ***H***, and (in ***I***) ***I***, ***J***, 50 μm.

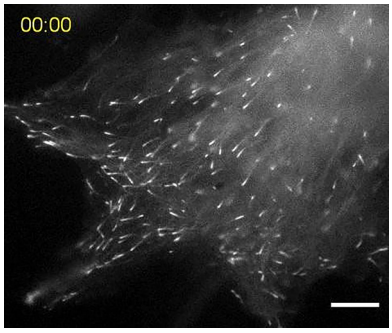

Movie 1. EB3-mNG overexpression in WT MEFs induced by lentivirus infection. MT dynamics were visualized after overexpression of EB3-mNG in WT MEFs. Representative time lapse movie was shown. Live cell imaging was collected every 200 ms for 1 min. Scale bar, 10 μm. [View online]

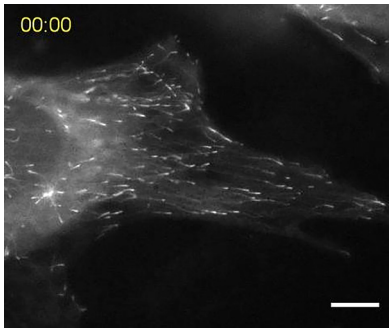

Movie 3. EB3-mNG overexpression in tau$^{-/-}$ MEFs induced by lentivirus infection. MT dynamics were visualized after overexpression of EB3-mNG in tau$^{-/-}$ MEFs. Representative time lapse movie was shown. Live cell imaging was collected every 200 ms for 1 min. Scale bar, 10 μm. [View online]

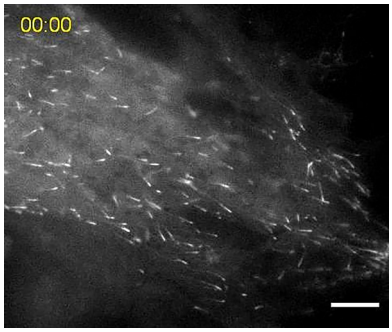

Movie 2. EB3-mNG overexpression in αSyn$^{-/-}$ MEFs induced by lentivirus infection. MT dynamics were visualized after overexpression of EB3-mNG in αSyn$^{-/-}$ MEFs. Representative time lapse movie was shown. Live cell imaging was collected every 200 ms for 1 min. Scale bar, 10 μm. [View online]

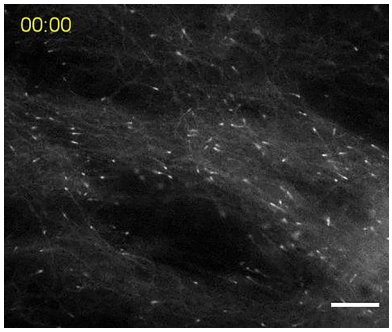

Movie 4. EB3-mNG overexpression in αSyn$^{-/-}$tau$^{-/-}$ MEFs induced by lentivirus infection. MT dynamics were visualized after overexpression of EB3-mNG in αSyn$^{-/-}$tau$^{-/-}$ MEFs. Representative time lapse movie was shown. Live cell imaging was collected every 200 ms for 1 min. Scale bar, 10 μm. [View online]

To examine whether the cortical architecture is affected in enlarged αSyn$^{-/-}$tau$^{-/-}$ cortices, P0 neocortices were immunostained with the layer-specific markers Cux1 and Ctip2. We observed that the numbers of deep layer Ctip2+ neurons and upper layer Cux1+ neurons were clearly increased in the αSyn$^{-/-}$tau$^{-/-}$ CP (Fig. 4*J–L*), suggesting that cortical hypertrophy is associated with enhanced neurogenesis.

MT dynamics is altered in αSyn$^{-/-}$tau$^{-/-}$ MEFs

αSyn and tau share a common function as MT regulators (Moussaud et al., 2014). MTs play essential roles in the proliferation and differentiation of NPCs (Conde and Cáceres, 2009). To analyze the effects of αSyn and tau on MT organization, we assessed the MT network in fibroblasts isolated from WT and KO embryos. MEFs did not display any morphologic abnormalities. However, after MT depolymerization via nocodazole treatment, we observed that newly extended MTs were shorter and less straight in αSyn$^{-/-}$tau$^{-/-}$ MEFs (Fig. 5*A–C*). We then investigated the effects on MT dynamics after overexpression of the plus end-binding protein EB3-mNG in the four genotypes of MEFs by lentiviral transduction. Compared with WT, MEFs derived from αSyn$^{-/-}$ or tau$^{-/-}$ showed a tendency of decrease in MT polymerization, whereas αSyn$^{-/-}$tau$^{-/-}$ MEFs exhibited a drastic decrease in MT elongation (Fig. 5*D*, Movies 1, 2, 3, 4). These results suggest that functional loss of αSyn and tau impairs MT reorganization and dynamics. The altered MT reorganization and dynamics provide a molecular basis for the abnormal proliferation and differentiation of NPCs in αSyn$^{-/-}$tau$^{-/-}$ mice.

G2 phase interkinetic nuclear migration was accelerated in αSyn$^{-/-}$tau$^{-/-}$ mice

RGCs are apicobasally elongated, and their nuclei and somata move vertically within the VZ in a cell cycle–dependent manner, a process called interkinetic nuclear migration (INM). Coupling of MT regulation with the cell cycle controls the timing of INM. This nuclear/somal movement is intimately linked to differentiation and neurogenesis (Miyata et al., 2014). To determine the effects of impaired MT stability and dynamics on neurogenesis, we traced cell cycle–dependent INM in WT and αSyn$^{-/-}$tau$^{-/-}$ cortical slices, through *in vivo* experiments. After coexpression of Lyn-EGFP and H_2B-RFP by IUE at E12, embryonic cerebral walls were isolated at E13 and subjected to slice culture and live imaging. Compared with WT RGCs, G2 phase nuclear/somal movements toward the apical surface were faster in αSyn$^{-/-}$tau$^{-/-}$ (Fig. 5*E*,*F*, Movies 5, 6). After 16 h of observation, 49.5% ± 3.87 and 75.3% ± 3.87 of the RGCs coelectroporated with Lyn-EGFP and H_2B-RFP had escaped from the VZ in WT and αSyn$^{-/-}$tau$^{-/-}$ slices, respectively (Fig. 5*G*,*H*). Additionally, 2 d after IUE at E12, almost all Lyn-EGFP and H_2B-RFP-coexpressing cells had reached the CP in the αSyn$^{-/-}$tau$^{-/-}$ E14 slices (Fig. 5*I*,*J*), emphasizing that accelerated neurogenesis occurred during the E12–E14 stage in the αSyn$^{-/-}$tau$^{-/-}$ group as shown in Figure 2. Collectively, these data indicate that the facilitated neurogenesis coupled with the accelerated INM during G2 phase led to an overproduction of early born neurons in αSyn$^{-/-}$tau$^{-/-}$ mice.

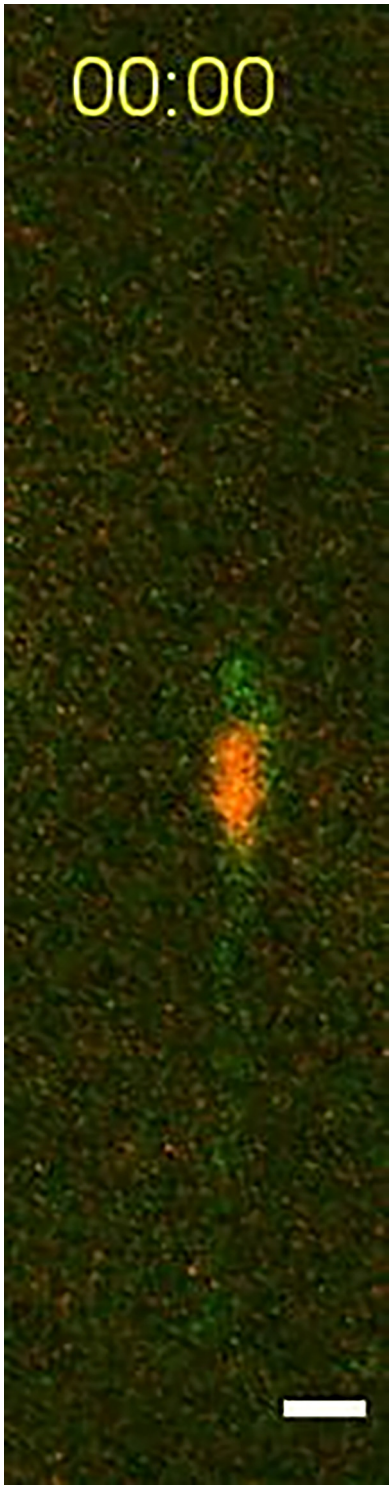

Movie 5. G2 phase INM in WT cerebral slices. Lyn-EGFP (cell membrane) and H_2B-RFP (cell nucleus) were electroporated into WT E12, and brain slice culture and apical INM during G2 phase were observed at E13. Scale bar, 20 μm. [View online]

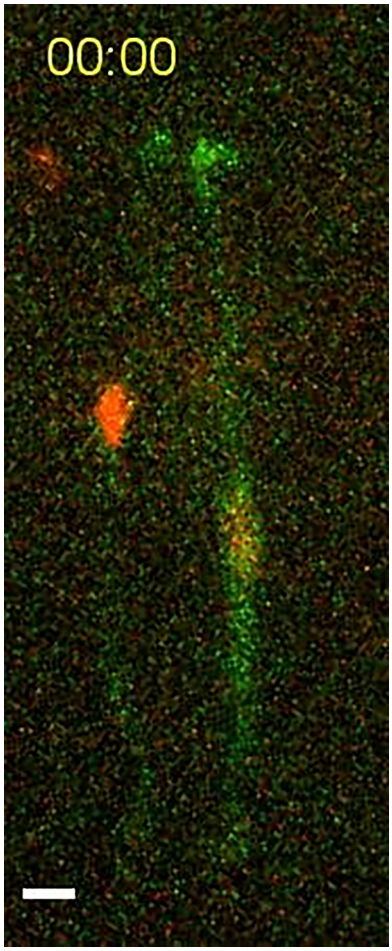

Movie 6. G2 phase INM in $\alpha Syn^{-/-}tau^{-/-}$ cerebral slices. Lyn-EGFP (cell membrane) and H_2B-RFP (cell nucleus) were electroporated into $\alpha Syn^{-/-}tau^{-/-}$ E12, and brain slice culture and apical INM during G2 phase were observed at E13. Scale bar, 20 μm. [View online]

Loss of αSyn and tau diminishes gliogenesis in the later stage of corticogenesis

Our results indicated that αSyn and tau play an essential role in neurogenesis through proper maintenance of NPCs. Loss of both αSyn and tau gave rise to premature neurogenesis at E11 and enhanced neurogenesis from E12, consequently resulting in a decrease in the number of RGCs at E15. In general, gliogenesis is followed by neurogenesis. Presumably, a reduction in NPCs can affect subsequent gliogenesis in the later embryonic stage. To confirm this hypothesis, we examined the behaviors of astrocytes and oligodendrocytes at P11. Consistent with the observations in the brains of 6-week-old mice, we observed a significant decrease in the cortical surface area at P11 $\alpha Syn^{-/-}tau^{-/-}$ mice (Fig. 6*A*, *B*). The cortical thickness was also compared after Tbr1 immunostaining. The thickness of cortical layers II–VI was clearly decreased in $\alpha Syn^{-/-}tau^{-/-}$ mice at P11 compared with that in WT and both genotypes of single-KO mice (Fig. 6*C*,*D*). In contrast, the Tbr1+ deep layer cell density in $\alpha Syn^{-/-}tau^{-/-}$ mice was higher than that of WT, $\alpha Syn^{-/-}$, and $tau^{-/-}$ mice (Fig. 6*C*, *E*). Neuronal death was also examined using an apoptosis marker, cleaved caspase-3, and no clear apoptotic cells were detected, even in $\alpha Syn^{-/-}tau^{-/-}$ mice (Fig. 6*F*,*G*). Consistent with this observation, no differences were found in the number of activated microglia (Iba1+; Fig. 6*H–J*), which normally respond to neuronal cell damage and remove the damaged cells by phagocytosis in the CNS. These results corroborate our finding that the later stage of cortical development was affected in $\alpha Syn^{-/-}tau^{-/-}$ cortices without apparent neuronal cell death.

We next examined P11 brain sections by using S100β, a marker of differentiated astrocytes, and Olig2, a marker of precursor and mature oligodendrocytes (Takebayashi et al., 2000). Compared with WT and both genotypes of single-KO mice, $\alpha Syn^{-/-}tau^{-/-}$ exhibited markedly decreased numbers of

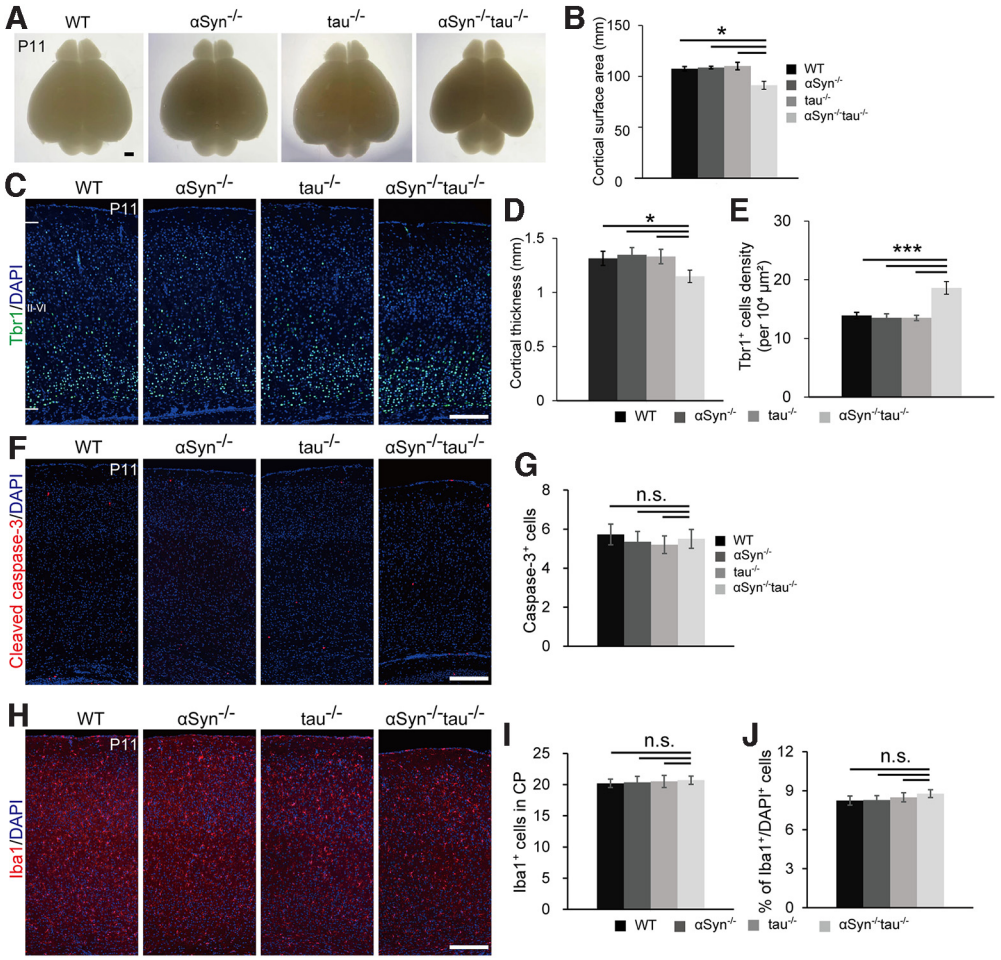

Figure 6. Brain size was reduced in $\alpha Syn^{-/-}tau^{-/-}$ mice. ***A***, ***B***, Comparison of brain size in P11 mice. Scale bar, 1 mm. ***C–E***, Quantification of the thickness of cortical layers II–VI (***D***) and the deep layer neuron density (***E***) at P11 after immunostaining for Tbr1 (green, ***C***). Scale bar, 200 μm. ***F–J***, Neuronal death was investigated with cleaved caspase-3 (***F, G***) and Iba1 (***H–J***) markers. Scale bar, 200 μm. The data are presented as mean ± SEM, $N = 3$ brains from three different litters for each genotype. The p values were calculated by one-way ANOVA with Tukey's *post hoc* test; n.s., not significant; *$p < 0.05$, ***$p < 0.001$.

S100β+ astrocytes in the CP and white matter (WM; Fig. 7*A–E*). Similarly, the numbers of Olig2+ oligodendrocytes were reduced in the CP and WM of $\alpha Syn^{-/-}tau^{-/-}$ mice (Fig. 7*F–J*). Furthermore, we examined the maturation of astrocytes and oligodendrocytes. The expression of GFAP, a mature and developing astrocyte marker (Yang and Wang, 2015), was examined by immunohistochemistry. The intensity of GFAP staining was significantly decreased in both the pial and protoplasmic regions in $\alpha Syn^{-/-}tau^{-/-}$ cortices (Fig. 8*A–C*). Mature oligodendrocytes were probed with an anti-myelin basic protein (MBP) antibody. Similar to findings in astrocytes, the density of MBP in oligodendrocytes was clearly decreased in the WM of $\alpha Syn^{-/-}tau^{-/-}$ mice at P11 (Fig. 8*D*,*E*).

To determine whether the diminished gliogenesis was attributable to a decrease in the number of IPCs, we immunostained E15 brain sections with an antibody against Ascl1, an IPC marker biased toward the oligodendrocyte lineage (Han et al., 2021). As we expected, the number of Ascl1+ IPCs was significantly reduced in E15 $\alpha Syn^{-/-}tau^{-/-}$ cortices (Fig. 8*F*). Collectively, these results indicate that the enhancement of early stage neurogenesis in $\alpha Syn^{-/-}tau^{-/-}$ mice affects subsequent gliogenesis. Furthermore, loss of αSyn and tau function impaired the expansion and maturation of astrocytes and oligodendrocytes in postnatal brains. This impairment may have contributed to the reduction of brain size in P11 and adult mice.

To determine the switch point of brain size, we first examined P7 cortices as expansion of astrocytes occurs during the first postnatal week (Clavreul et al., 2019). P7 cortices were immunostained with Cux1 and Ctip2 markers, and the cortical thickness was compared. The thickness of cortical layers II-VI in $\alpha Syn^{-/-}tau^{-/-}$ mice at P7 was comparable to that in WT and two types of single-KO mice (Fig. 9*A*,*B*). Conversely, $\alpha Syn^{-/-}tau^{-/-}$ mice displayed a significant increase in the number of upper layer Cux1+ neurons, but not deep layer Ctip2+ neurons (Fig. 9*A*,*C*,*D*). Moreover, increased neuronal cell densities in the upper and deep layers were confirmed in $\alpha Syn^{-/-}tau^{-/-}$ mice (Fig. 9*A*,*E*,*F*). These results prompted us to further examine the behavior of neuronal cells in cortices from P11 and 6-week-old mice. Similarly, we confirmed an increase in the number of upper layer Cux1+ neurons in $\alpha Syn^{-/-}tau^{-/-}$ mice at P11 (Fig. 9*G–I*), with higher neuronal cell densities in both the upper and deep layers (Fig. 9*G*,*J*,*K*). Consistent with the P7 and P11 cortices, increases in the neuronal cell densities in both the upper and deep layers were detected in 6-week-old $\alpha Syn^{-/-}tau^{-/-}$ mice (Figs. 1*D*, 9*L*,*M*). These results strongly suggest that the reduction in brain size in adult $\alpha Syn^{-/-}tau^{-/-}$ mice is potentially because of the downregulation of gliogenesis and expansion and maturation of microglial cells without neuronal loss.

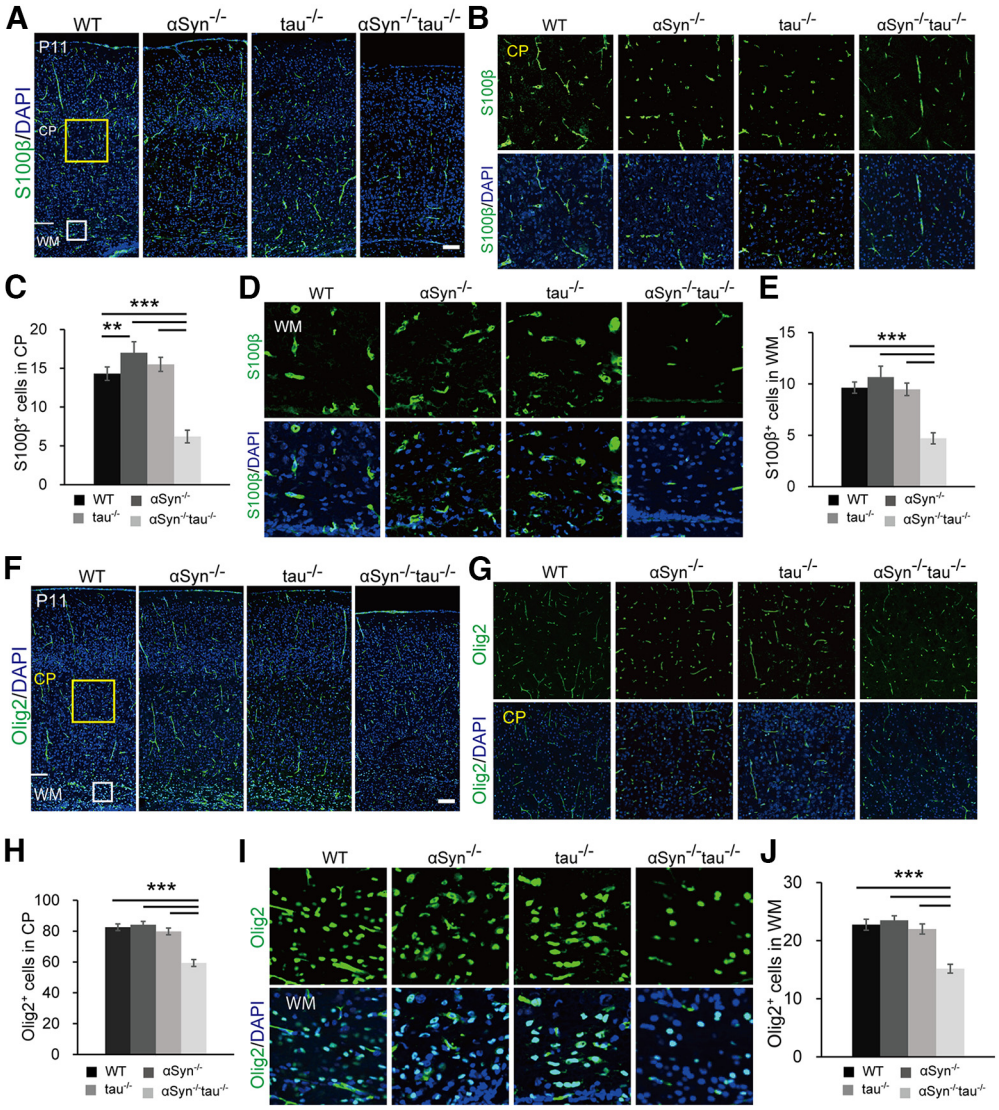

Figure 7. Astrogenesis and oligodendrogenesis were diminished in $\alpha Syn^{-/-}tau^{-/-}$ mice. ***A–E***, Statistical analyses of astrocytes in P11 cortices. P11 brain sections were stained for S100β (green, ***A***) and quantification of S100β + astrocytes in the CP (***C***) and WM (***E***) was performed per 300 μm column. Each area surrounded by a yellow rectangle (CP) is enlarged and shown in ***B***, and the white boxed area (WM) is shown in ***D***. Scale bar, 100 μm. ***F–J***, Quantification of oligodendrocytes with the marker Olig2 at P11. P11 brain sections were immunostained with anti-Olig2 antibody (green, ***F***), and quantification of Olig2+ oligodendrocytes in the CP (***H***) and WM (***J***) was performed per 300 μm column. Each area in the yellow box is shown in ***G***, and the white boxed area is shown in ***I***. Scale bar, 100 μm. The quantitative data are presented as the mean ± SEM, $N = 3$ brains from three different litters for each genotype. The p values were calculated by one-way ANOVA with Tukey's *post hoc* test; $^{**}p < 0.01$, $^{***}p < 0.001$.

Discussion

αSyn and tau are abundant neuronal MAPs, and their abnormal intracellular aggregates have been linked to various neurodegenerative disorders (Vasili et al., 2019; Vacchi et al., 2020). Despite extensive endeavors, their physiological roles remain elusive because of the subtle phenotypes in mice with knock-out of the individual genes (Ke et al., 2012; Pathak et al., 2017). In this study, we demonstrated that αSyn and tau cooperatively play multiple developmental roles in a stage-dependent manner.

Cortical neurons and macroglial cells arise from a common proliferative RGCs (Rowitch and Kriegstein, 2010). Before the onset of neurogenesis, RGCs undergo symmetric cell division to produce two daughter cells that adopt the progenitor fate (Rakic, 1982; Taverna et al., 2014). We show here that loss of αSyn and tau affected the balance between proliferative and neurogenic divisions of RGCs, resulting in an overproduction of early born neurons. This led to an enlarged brain in $\alpha Syn^{-/-}tau^{-/-}$ embryos. The finding of facilitated neurogenesis was supported by the *in utero* electroporation experiments using E12–E14 cerebral slices, in which $\alpha Syn^{-/-}tau^{-/-}$ G2 phase nuclear/somal movements became faster at E13, and almost all cells coelectroporated with Lyn-EGFP and H_2B-RFP had escaped from the VZ to the neocortex at E14. Consistent with this, an increase in the number of postmitotic neurons and an increased neocortical thickness were observed during the embryonic stage that was retained until the neonatal stage in $\alpha Syn^{-/-}tau^{-/-}$ mice. Notably, enhancement of neurogenesis led to an increase in cortical thickness, without causing histologic layer defects, indicating that αSyn and tau are cooperatively involved in the maintenance of NPCs, but not postmitotic neuronal migration during cortical lamination.

Differentiation of RGCs toward IPCs was also facilitated in E12 embryos but decreased in E14 $\alpha Syn^{-/-}tau^{-/-}$ mice. Moreover, a reduction in the RGC pool was found at E15.

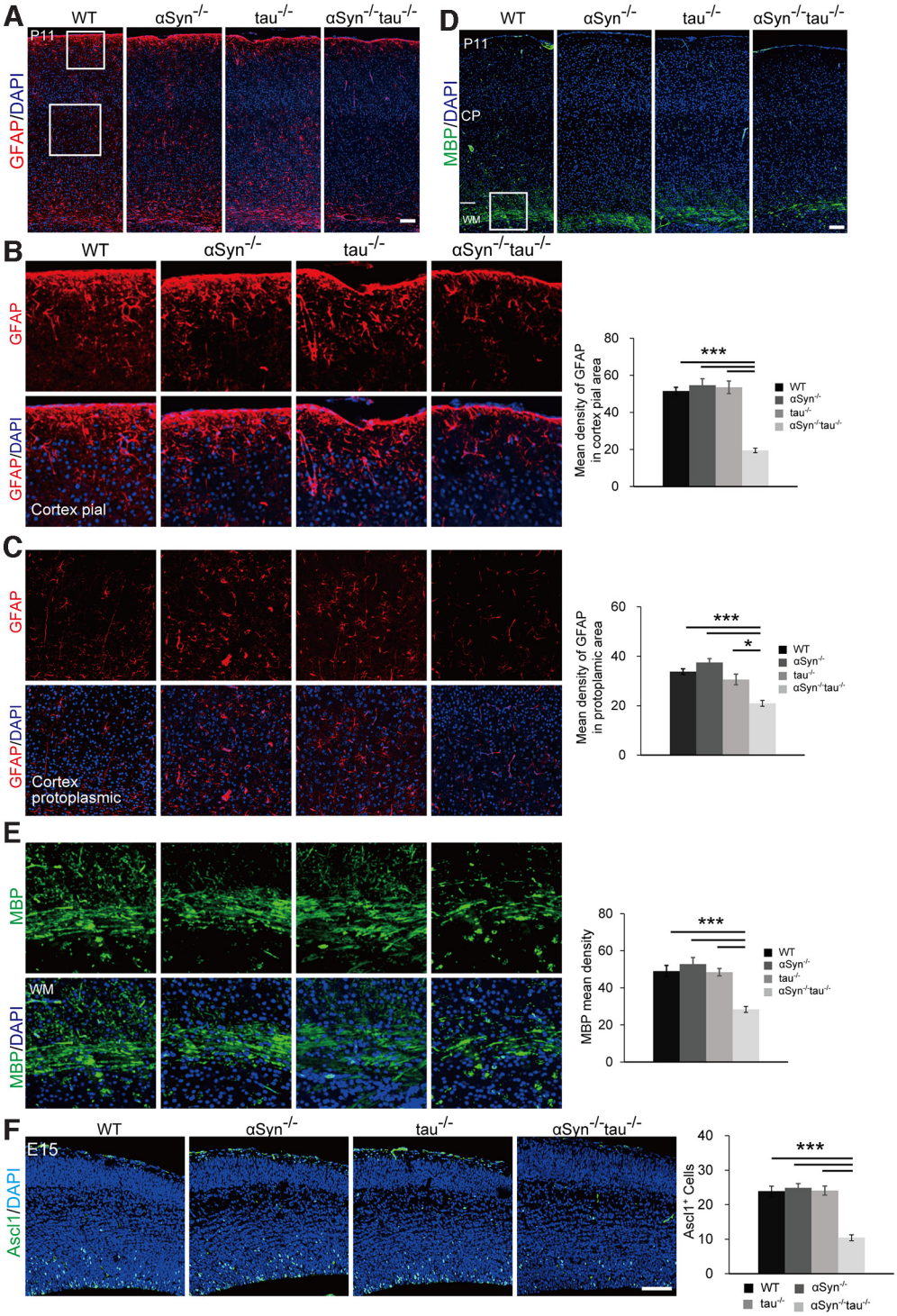

Figure 8. Downregulated maturation of astrocytes and oligodendrocytes was detected in αSyn$^{-/-}$tau$^{-/-}$ mice. ***A–C***, Astrocyte maturation was confirmed by GFAP immunostaining at P11. The areas surrounded by a white rectangle are enlarged and shown in ***B*** and ***C***. The GFAP density in both the pial and protoplasmic areas of the cortex were quantified. ***D***, ***E***, Oligodendrocyte maturation was confirmed by MBP immunostaining at P11. The white boxed area is enlarged and shown in ***E***. ***F***, Differentiated IPCs at E15 analyzed by staining for Ascl1, a basal progenitor cell marker biased toward oligodendrogenesis. The cells were counted in a 100 μm column. Mean MBP densities in WM were measured in a 50 $\times$ 50 μm^2 area. The quantitative data are presented as mean $\pm$ SEM, $N = 3$ brains from three different litters for each genotype. The p values were calculated by one-way ANOVA with Tukey's *post hoc* test; *$p < 0.05$, ***$p < 0.001$. Scale bars: (in ***A***) ***A–C***, (in ***D***) ***D***, ***E***, 100 μm; (in ***F***), 50 μm.

Presumably, the premature and facilitated neurogenesis at the early embryonic stage caused excess exhaustion of RGCs in αSyn$^{-/-}$tau$^{-/-}$ mice. As we expected, the reductions in the RGC and IPC pools in αSyn$^{-/-}$tau$^{-/-}$ cortices also affected subsequent gliogenesis at later embryonic stage, and this effect was accompanied by impaired expansion and maturation of astrocytes and oligodendrocytes in the postnatal brain. Clavreul et al. (2019) reported that expansion of astrocytes occurs during the first postnatal week, and P7–P21 is the maturation phase during which each astrocyte increases the volume and complexity of their processes. Accordingly, at P11 and 6 weeks of age, αSyn$^{-/-}$tau$^{-/-}$ mice displayed smaller brains than WT and two types of single-

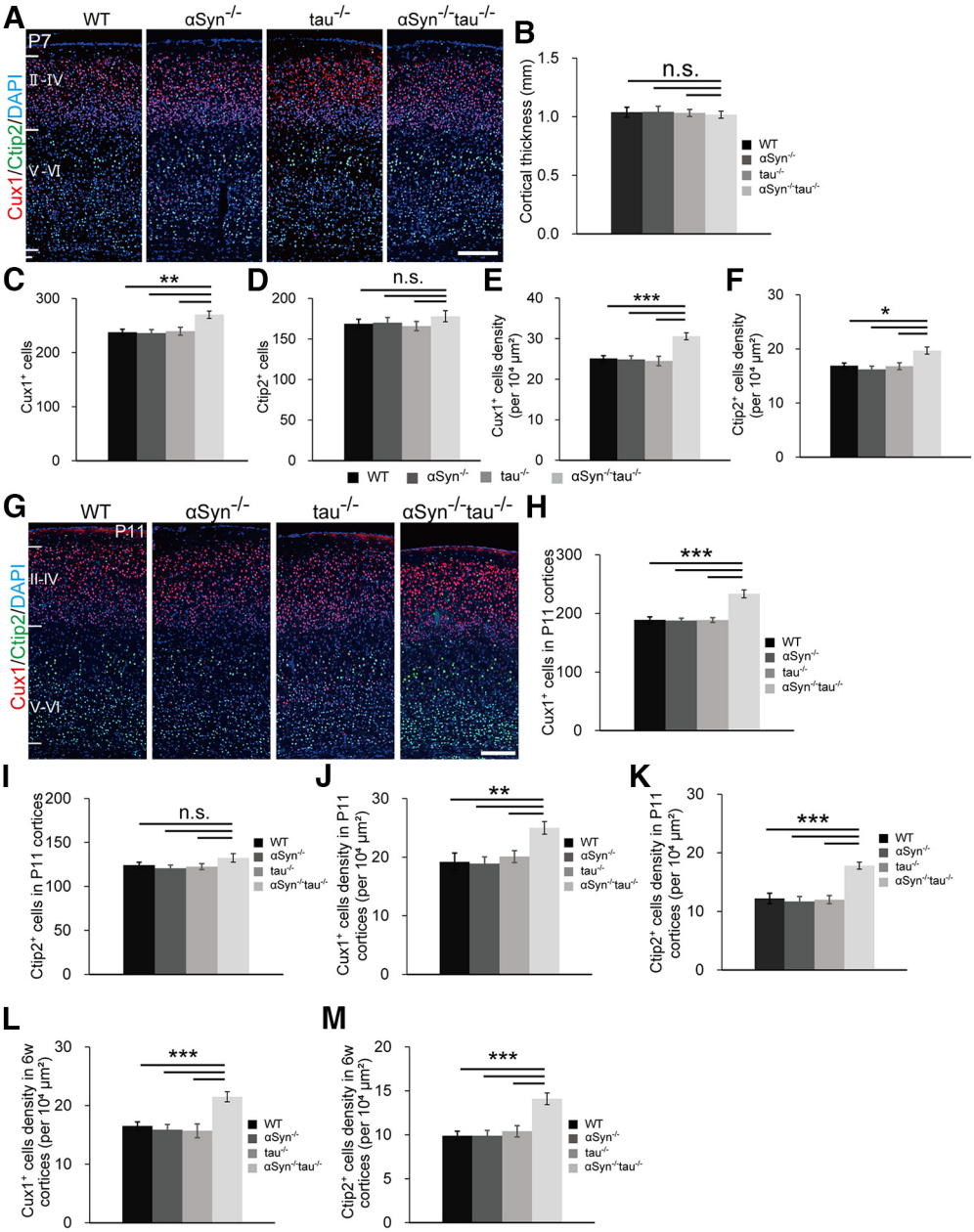

Figure 9. The downregulated brain size in $\alpha Syn^{-/-}tau^{-/-}$ mice was caused by diminished gliogenesis. ***A–F***, Quantification of neuronal cells in P7 cortices. Cortical neurons were probed with Cux1 (red) and Ctip2 (green) markers (***A***), and the thickness of layers II–VI (***B***), the neuron numbers (***C***, ***D***) and the cell densities (***E***, ***F***) were quantified. The cells were counted in a 300 μm column, and the cell densities were calculated in a 100 × 100 μm^2 area. Scale bar, 200 μm. ***G–K***, Quantification of neuronal cells in P11 cortices. Cortical neurons were probed with Cux1 (red) and Ctip2 (green) markers (***G***), and the neuron numbers (***H***, ***I***) and cell densities (***J***, ***K***) were quantified. The cells were counted in a 300 μm column. Scale bar, 200 μm. ***L***, ***M***, The Cux1+ neuron density in layers II–IV (***L***) and Ctip2+ neuron density in layers V–VI (***M***) were quantified in the cortices from the 6-week-old mice (Fig. 1*D*). The quantitative data are presented as mean ± SEM, $N = 3$ brains from three separate litters for each genotype. The p values were calculated by one-way ANOVA with Tukey's *post hoc* test; n.s., not significant; $^*p < 0.05$, $^{**}p < 0.01$, $^{***}p < 0.001$.

KO mice, accompanied by increased neuronal cell densities in the upper and deep layers, without neuronal cell death. Notably, astrocytes interact with multiple types of cells, including neurons, glial cells, and endothelial cells in blood vessels, whereas mature oligodendrocytes generate a myelin sheath that surrounds and insulates axons and facilitates the transmission of neural impulses in the CNS (Hartline and Colman, 2007; Chang et al., 2016). Emerging evidence suggests that the loss of beneficial roles of glial cells can contribute to neurodegenerative conditions (Tremblay et al., 2019). Dysregulation of gliogenesis and their expansion and maturation caused by deletion of αSyn and tau provide important insights into elucidating pathogeneses of neurodegenerative diseases including PD and multiple system atrophy.

MT organization plays pivotal roles during proliferation and differentiation of NPCs, including the cell cycle–dependent INM (Spear and Erickson, 2012; Cooper, 2013; Lasser et al., 2018). αSyn and tau share a common feature as neuronal MAPs. We found that absence of αSyn and tau diminished MT reorganization and dynamics. Conversely, G2 phase INM velocity was clearly accelerated in $\alpha Syn^{-/-}tau^{-/-}$ brain slices, and neurogenesis was significantly enhanced from the early embryonic stage. Previous work revealed that mutation in a microtubule-motor-associated protein dynactin perturbs INM and

accelerated retinal neurogenesis in the zebrafish (Del Bene et al., 2008). Furthermore, Notch signaling plays crucial roles in the proliferation and differentiation of NPCs (Mase et al., 2021). In $\alpha Syn^{-/-}tau^{-/-}$, we also established that Notch signaling was reduced during neurogenesis. Downregulation of Notch target genes leads to upregulation of proneural genes and neuronal differentiation (Kawaguchi et al., 2008). In line with this, increased numbers of Ngn2-expressing IPCs were detected in E12 $\alpha Syn^{-/-}tau^{-/-}$ cortices. Collectively, the data indicate that the precocious and the facilitated neurogenesis at early embryonic stage in $\alpha Syn^{-/-}tau^{-/-}$ brains is probably because of the reduction in Notch signaling and accelerated INM. Both intracellular Notch signaling conduction and INM depend on microtubule-associated-motor proteins (Del Bene et al., 2008; Tsai et al., 2010; Hu et al., 2013). Presumably, diminished MT reorganization perturbs conduction of Notch signaling and cell cycle–dependent INM. More detailed studies are needed to better understand the mechanisms underlying the facilitated proliferation and differentiation of NPCs in $\alpha Syn^{-/-}tau^{-/-}$ mice.

Intracellular codeposition of pathologic αSyn and tau has been linked to many neurologic disorders, including AD and PD (Moussaud et al., 2014; Li et al., 2016; Henderson et al., 2019). Furthermore, cross-seeding of αSyn and tau has been investigated *in vitro* and *in vivo* (Li et al., 2016; Lu et al., 2020). For this reason, the interaction between αSyn and tau is considered to develop neurodegenerative disorders. Here, we revealed previously unrecognized functional cross talk between αSyn and tau during neurogenesis and gliogenesis. Our findings might provide new mechanistic insights and expand the therapeutic opportunities for neurodegenerative diseases caused by aberrant αSyn and/or tau.

References

Abeliovich A, Schmitz Y, Fariñas I, Choi-Lundberg D, Ho WH, Castillo PE, Shinsky N, Verdugo JM, Armanini M, Ryan A, Hynes M, Phillips H, Sulzer D, Rosenthal A (2000) Mice lacking alpha-synuclein display functional deficits in the nigrostriatal dopamine system. Neuron 25:239–252.

Alim MA, Ma QL, Takeda K, Aizawa T, Matsubara M, Nakamura M, Asada A, Saito T, Kaji H, Yoshii M, Hisanaga S, Ueda K (2004) Demonstration of a role for alpha-synuclein as a functional microtubule-associated protein. J Alzheimers Dis 6:435–442.

Arlotta P, Molyneaux BJ, Chen J, Inoue J, Kominami R, Macklis JD (2005) Neuronal subtype-specific genes that control corticospinal motor neuron development in vivo. Neuron 45:207–221.

Bond AM, Berg DA, Lee S, Garcia-Epelboim AS, Adusumilli VS, Ming GL, Song H (2020) Differential timing and coordination of neurogenesis and astrogenesis in developing mouse hippocampal subregions. Brain sciences 10:909.

Calogero AM, Mazzetti S, Pezzoli G, Cappelletti G (2019) Neuronal microtubules and proteins linked to Parkinson's disease: a relevant interaction? Biol Chem 400:1099–1112.

Cartelli D, et al. (2016) α-Synuclein is a novel microtubule dynamase. Sci Rep 6:33289.

Chang CW, Shao E, Mucke L (2021) Tau: enabler of diverse brain disorders and target of rapidly evolving therapeutic strategies. Science 371.

Chang KJ, Redmond SA, Chan JR (2016) Remodeling myelination: implications for mechanisms of neural plasticity. Nat Neurosci 19:190–197.

Chen L, Jin J, Davis J, Zhou Y, Wang Y, Liu J, Lockhart PJ, Zhang J (2007) Oligomeric alpha-synuclein inhibits tubulin polymerization. Biochem Biophys Res Commun 356:548–553.

Clavreul S, Abdeladim L, Hernández-Garzón E, Niculescu D, Durand J, Ieng SH, Barry R, Bonvento G, Beaurepaire E, Livet J, Loulier K (2019) Cortical astrocytes develop in a plastic manner at both clonal and cellular levels. Nat Commun 10:4884.

Cleveland DW, Hwo SY, Kirschner MW (1977) Purification of tau, a microtubule-associated protein that induces assembly of microtubules from purified tubulin. J Mol Biol 116:207–225.

Conde C, Cáceres A (2009) Microtubule assembly, organization and dynamics in axons and dendrites. Nat Rev Neurosci 10:319–332.

Cooper JA (2013) Cell biology in neuroscience: mechanisms of cell migration in the nervous system. J Cell Biol 202:725–734.

Del Bene F, Wehman AM, Link BA, Baier H (2008) Regulation of neurogenesis by interkinetic nuclear migration through an apical-basal notch gradient. Cell 134:1055–1065.

Drubin DG, Kirschner MW (1986) Tau protein function in living cells. J Cell Biol 103:2739–2746.

Fiock KL, Smalley ME, Crary JF, Pasca AM, Hefti MM (2020) Increased tau expression correlates with neuronal maturation in the developing human cerebral cortex. eNeuro 7:ENEURO.0058-20.2020.

Forman MS, Schmidt ML, Kasturi S, Perl DP, Lee VM, Trojanowski JQ (2002) Tau and alpha-synuclein pathology in amygdala of Parkinsonism-dementia complex patients of Guam. Am J Pathol 160:1725–1731.

Greig LC, Woodworth MB, Galazo MJ, Padmanabhan H, Macklis JD (2013) Molecular logic of neocortical projection neuron specification, development and diversity. Nat Rev Neurosci 14:755–769.

Han S, Dennis DJ, Balakrishnan A, Dixit R, Britz O, Zinyk D, Touahri Y, Olender T, Brand M, Guillemot F, Kurrasch D, Schuurmans C (2018) A non-canonical role for the proneural gene Neurog1 as a negative regulator of neocortical neurogenesis. Development 145: dev157719.

Han S, et al. (2021) Proneural genes define ground-state rules to regulate neurogenic patterning and cortical folding. Neuron 109: 2847–2863.e11.

Harada A, Oguchi K, Okabe S, Kuno J, Terada S, Ohshima T, Sato-Yoshitake R, Takei Y, Noda T, Hirokawa N (1994) Altered microtubule organization in small-calibre axons of mice lacking tau protein. Nature 369:488–491.

Hartline DK, Colman DR (2007) Rapid conduction and the evolution of giant axons and myelinated fibers. Curr Biol 17:R29–R35.

Henderson MX, Trojanowski JQ, Lee VM-Y (2019) α-Synuclein pathology in Parkinson's disease and related α-synucleinopathies. Neurosci Lett 709:134316.

Hsu LJ, Mallory M, Xia Y, Veinbergs I, Hashimoto M, Yoshimoto M, Thal LJ, Saitoh T, Masliah E (1998) Expression pattern of synucleins (non-Abeta component of Alzheimer's disease amyloid precursor protein/alpha-synuclein) during murine brain development. J Neurochem 71:338–344.

Hu DJ, Baffet AD, Nayak T, Akhmanova A, Doye V, Vallee RB (2013) Dynein recruitment to nuclear pores activates apical nuclear migration and mitotic entry in brain progenitor cells. Cell 154:1300–1313.

Ishizawa T, Mattila P, Davies P, Wang D, Dickson DW (2003) Colocalization of tau and alpha-synuclein epitopes in Lewy bodies. J Neuropathol Exp Neurol 62:389–397.

Jin M, Pomp O, Shinoda T, Toba S, Torisawa T, Furuta K, Oiwa K, Yasunaga T, Kitagawa D, Matsumura S, Miyata T, Tan TT, Reversade B, Hirotsune S (2017) Katanin p80, NuMA and cytoplasmic dynein cooperate to control microtubule dynamics. Sci Rep 7:39902.

Kawaguchi D, Yoshimatsu T, Hozumi K, Gotoh Y (2008) Selection of differentiating cells by different levels of delta-like 1 among neural precursor cells in the developing mouse telencephalon. Development 135:3849–3858.

Ke YD, Suchowerska AK, van der Hoven J, De Silva DM, Wu CW, van Eersel J, Ittner A, Ittner LM (2012) Lessons from tau-deficient mice. Int J Alzheimers Dis 2012:873270.

Kopan R, Ilagan MX (2009) The canonical Notch signaling pathway: unfolding the activation mechanism. Cell 137:216–233.

Lasser M, Tiber J, Lowery LA (2018) The role of the microtubule cytoskeleton in neurodevelopmental disorders. Front Cell Neurosci 12:165.

Li X, James S, Lei P (2016) Interactions between α-synuclein and tau protein: implications to neurodegenerative disorders. J Mol Neurosci 60:298–304.

Lu J, Zhang S, Ma X, Jia C, Liu Z, Huang C, Liu C, Li D (2020) Structural basis of the interplay between α-synuclein and Tau in regulating pathological amyloid aggregation. J Biol Chem 295:7470–7480.

Maroteaux L, Campanelli JT, Scheller RH (1988) Synuclein: a neuron-specific protein localized to the nucleus and presynaptic nerve terminal. J Neurosci 8:2804–2815.

Mase S, Shitamukai A, Wu Q, Morimoto M, Gridley T, Matsuzaki F (2021) Notch1 and Notch2 collaboratively maintain radial glial cells in mouse neurogenesis. Neurosci Res 170:122–132.

Millecamps S, Julien JP (2013) Axonal transport deficits and neurodegenerative diseases. Nat Rev Neurosci 14:161–176.

Miyata T, Kawaguchi A, Saito K, Kawano M, Muto T, Ogawa M (2004) Asymmetric production of surface-dividing and non-surface-dividing cortical progenitor cells. Development 131:3133–3145.

Miyata T, Okamoto M, Shinoda T, Kawaguchi A (2014) Interkinetic nuclear migration generates and opposes ventricular-zone crowding: insight into tissue mechanics. Front Cell Neurosci 8:473.

Moussaud S, Jones DR, Moussaud-Lamodière EL, Delenclos M, Ross OA, McLean PJ (2014) Alpha-synuclein and tau: teammates in neurodegeneration? Mol Neurodegener 9:43.

Muramatsu K, Hashimoto Y, Uemura T, Kunii M, Harada R, Sato T, Morikawa A, Harada A (2008) Neuron-specific recombination by Cre recombinase inserted into the murine tau locus. Biochem Biophys Res Commun 370:419–423.

Nieto M, Monuki ES, Tang H, Imitola J, Haubst N, Khoury SJ, Cunningham J, Gotz M, Walsh CA (2004) Expression of Cux-1 and Cux-2 in the subventricular zone and upper layers II–IV of the cerebral cortex. J Comp Neurol 479:168–180.

Okamoto M, et al. (2013) TAG-1-assisted progenitor elongation streamlines nuclear migration to optimize subapical crowding. Nat Neurosci 16:1556–1566.

Pathak D, Berthet A, Bendor JT, Yu K, Sellnow RC, Orr AL, Nguyen MK, Edwards RH, Manfredsson FP, Nakamura K (2017) Loss of α-synuclein does not affect mitochondrial bioenergetics in rodent neurons. eNeuro 4: ENEURO.0216-16.2017.

Poirier K, et al. (2007) Large spectrum of lissencephaly and pachygyria phenotypes resulting from de novo missense mutations in tubulin alpha 1A (TUBA1A). Hum Mutat 28:1055–1064.

Polymeropoulos MH, Lavedan C, Leroy E, Ide SE, Dehejia A, Dutra A, Pike B, Root H, Rubenstein J, Boyer R, Stenroos ES, Chandrasekharappa S, Athanassiadou A, Papapetropoulos T, Johnson WG, Lazzarini AM, Duvoisin RC, Di Iorio G, Golbe LI, Nussbaum RL (1997) Mutation in the alpha-synuclein gene identified in families with Parkinson's disease. Science 276:2045–2047.

Prots I, Grosch J, Brazdis RM, Simmnacher K, Veber V, Havlicek S, Hannappel C, Krach F, Krumbiegel M, Schütz O, Reis A, Wrasidlo W, Galasko DR, Groemer TW, Masliah E, Schlötzer-Schrehardt U, Xiang W, Winkler J, Winner B (2018) α-Synuclein oligomers induce early axonal dysfunction in human iPSC-based models of synucleinopathies. Proc Natl Acad Sci U S A 115:7813–7818.

Qiang L, Yu W, Andreadis A, Luo M, Baas PW (2006) Tau protects microtubules in the axon from severing by katanin. J Neurosci 26:3120–3129.

Rakic P (1982) Early developmental events: cell lineages, acquisition of neuronal positions, and areal and laminar development. Neurosci Res Program Bull 20:439–451.

Rowitch DH, Kriegstein AR (2010) Developmental genetics of vertebrate glial-cell specification. Nature 468:214–222.

Shafiq M, Zafar S, Younas N, Noor A, Puig B, Altmeppen HC, Schmitz M, Matschke J, Ferrer I, Glatzel M, Zerr I (2021) Prion protein oligomers cause neuronal cytoskeletal damage in rapidly progressive Alzheimer's disease. Mol Neurodegener 16:11.

Shinoda T, Nagasaka A, Inoue Y, Higuchi R, Minami Y, Kato K, Suzuki M, Kondo T, Kawaue T, Saito K, Ueno N, Fukazawa Y, Nagayama M, Miura T, Adachi T, Miyata T (2018) Elasticity-based boosting of neuroepithelial nucleokinesis via indirect energy transfer from mother to daughter. PLoS Biol 16:e2004426.

Sleigh JN, Rossor AM, Fellows AD, Tosolini AP, Schiavo G (2019) Axonal transport and neurological disease. Nat Rev Neurol 15:691–703.

Spear PC, Erickson CA (2012) Interkinetic nuclear migration: a mysterious process in search of a function. Dev Growth Differ 54:306–316.

Takebayashi H, Yoshida S, Sugimori M, Kosako H, Kominami R, Nakafuku M, Nabeshima Y (2000) Dynamic expression of basic helix-loop-helix Olig family members: implication of Olig2 in neuron and oligodendrocyte differentiation and identification of a new member, Olig3. Mech Dev 99:143–148.

Taverna E, Götz M, Huttner WB (2014) The cell biology of neurogenesis: toward an understanding of the development and evolution of the neocortex. Annu Rev Cell Dev Biol 30:465–502.

Toba S, Jin M, Yamada M, Kumamoto K, Matsumoto S, Yasunaga T, Fukunaga Y, Miyazawa A, Fujita S, Itoh K, Fushiki S, Kojima H, Wanibuchi H, Arai Y, Nagai T, Hirotsune S (2017) Alpha-synuclein facilitates to form short unconventional microtubules that have a unique function in the axonal transport. Sci Rep 7:16386.

Tremblay ME, Cookson MR, Civiero L (2019) Glial phagocytic clearance in Parkinson's disease. Mol Neurodegener 14:16.

Tsai JW, Lian WN, Kemal S, Kriegstein AR, Vallee RB (2010) Kinesin 3 and cytoplasmic dynein mediate interkinetic nuclear migration in neural stem cells. Nat Neurosci 13:1463–1471.

Vacchi E, Kaelin-Lang A, Melli G (2020) Tau and alpha synuclein synergistic effect in neurodegenerative diseases: when the periphery is the core. IJMS 21:5030.

Vasili E, Dominguez-Meijide A, Outeiro TF (2019) Spreading of α-synuclein and tau: a systematic comparison of the mechanisms involved. Front Mol Neurosci 12:107.

Weinreb PH, Zhen W, Poon AW, Conway KA, Lansbury PT Jr (1996) NACP, a protein implicated in Alzheimer's disease and learning, is natively unfolded. Biochemistry 35:13709–13715.

Yang Z, Wang KK (2015) Glial fibrillary acidic protein: from intermediate filament assembly and gliosis to neurobiomarker. Trends Neurosci 38: 364–374.